Pontificia Universidad Católica de Chile
Faculty of Physics
Institute of Astrophysics

The consistency of chemical clocks among coeval stars

by

Francisca Espinoza Rojas

Thesis submitted to the Faculty of Physics
of Pontificia Universidad Católica de Chile,
one of the requirements to qualify for the
academic Master's degree in Astrophysics

Supervisor	:	Dr. Julio Chanamé (PUC, Chile)
Co-supervisor	:	Dr. Paula Jofré (UDP, Chile)
Committee	:	Dr. Márcio Catelan (PUC, Chile)
		Dr. Melissa Ness (Columbia University, USA)

September, 2021

Santiago, Chile

©2021, Francisca Espinoza Rojas
The total or partial reproduction is authorized, for academic purposes, by any means or procedure, including the bibliographic citation of the document.

"We are all time travellers, journeying together into the future. But let us work together to make that future a place we want to visit.

Be brave, be curious, be determined, overcome the odds. It can be done."

– Stephen Hawking, Brief answers to the big questions (2018).

Acknowledgments

To my parents, for being an unconditional support during my life and in all the decisions I have made. For listening to me, even when it came to crazy astronomical things that they probably did not understand much; they always listened with a smile on their faces and the clear intention to learn. For always believing in me, and for pushing me to do my best, always dreaming big. Without you I would be nothing.

To my dearest friends, my brothers from another mother, Joaquín, Hernán, Patricio and Ignacio, whom I keep as the greatest gifts that university life has given me. Thank you for always being there, for all the amazing experiences we have live together, for always making me smile in moments of despair, for listening and helping me to see life in a different way. I hope that life always brings you a lot of happiness and fulfillment. Also I want to thank to Carolina, Álvaro, Cristóbal, Juan, and all my professors and colleagues from the Institute of Astrophysics, specially to Claudia, Alexandra, Victor, and Manuel from my team work. Thank you for all your support, help and life lessons, for the interesting discussions and hallway talks. You have been a great source of inspiration, motivation, and the reason why I have enjoyed academic life during these years.

And as the saying goes, the best for last. To my dear advisors, Julio Chanamé and Paula Jofré, for their dedication and for all the time they have spent guiding me and teaching me over the years. Thank you for your trust, for opening the doors to work with you, for giving me the space to develop my ideas, and for helping me to believe in myself. You were very supportive during these particularly challenging two years, when things turned upside down and it was difficult to find any kind of motivation to work. I never imagined that I would have to do my master's degree remotely, without being able to share with you in person on a daily or weekly basis. Thanks to you, this project managed to be a very enriching experience, both intellectually and personally, despite the adversities. Thanks for your advice and for all the laughs shared. I feel fortunate and grateful to have you as mentors.

Thanks to everyone that has been involved in this. I am indebted to you all.

Abstract

The abundance ratios of some chemical species have been found to correlate with stellar age, leading to the possibility of using measurements of abundances in stellar atmospheres as age indicators thanks to the Galactic chemical evolution. These *chemical clocks* have been calibrated with solar-twins, open clusters and red giants, however, how effective they are in identifying coeval systems has not been tested for populations that sample a broader parameter space. In that sense, wide binary systems are the perfect objects to assess the applications of chemical clocks, because their components have a common origin and are separated by great distances, so they should not interact with each other, and their abundances and ages are expected to be consistent. In this thesis, I determined the abundances of a sample of 5 wide binaries and collected data for other 31 systems from the literature in order to test the applicability of chemical clocks. I found that wide binaries have more consistent abundances than random pairs. I also found that chemical clocks are even more consistent among the components of wide binaries than their [X/Fe] ratios. Not only that, but the special case of the pair HIP 34426/HIP 34407 would indicate that chemical clocks are consistent for coeval stars even when their abundances are not. Finally, given the evidence that chemical clocks trace information about stellar birthplaces and chemical evolution, I briefly studied their benefits for chemical tagging by using them to reconstruct a sample of 3 open clusters, and found that chemical clocks do not improve the identification of the cluster's members, but could be used for decontamination. Despite this, the results are limited by the age range of the sample, and there is still much work that could be done to better evaluate this idea and find more applications for chemical clocks.

Contents

Chapter 1

Introduction

Stars are among the most important components of the baryonic Universe since they are the fundamental building blocks of huge structures like galaxies. Moreover, stars are the main responsible of the galactic chemical evolution given that most of the elements that we know are formed inside of them or during their final evolutionary stages (i.e. supernovae) through different nucleosynthetic processes. Then, these elements are released into the interstellar medium (ISM) and consequently enrich the gas, which in periods of millions of years is going to form other stars that will continue with this cycle.

The determination of chemical abundances from stellar spectra is therefore a pathway to unveil the chemical formation and evolution of our Galaxy, because they retain important information about the unique patterns of the elements produced over time, strongly depending on the mass and metallicity of their progenitor stars. Since stars of different masses have different lifetimes, the enrichment of ISM due to each nucleosynthetic process has different timescales.

Some nucleosynthetic families are the α-elements, Fe-peak, light/odd-Z and neutron capture elements. O, Mg, Si, Ca and Ti are α-capture elements, and are mostly produced at the interiors of evolved massive stars ($M > 10M_{\odot}$) through the successive fusion of helium nuclei ("α particle"). Then they are released by Type II supernovae, enriching the ISM within short timescales ($< 10^{-2}$ Gyr) and becoming overabundant in compari-

son to other elements at early stages of the Galaxy evolution. As time progresses, Type Ia supernovae start to take place and Fe-peak elements ($21 \leq Z \leq 30$) like Fe, Cr, Mn, Co, Ni and Zn are produced over longer timescales ($\sim$ 1 Gyr)(Spina et al., 2016), thus the relative abundance [α/Fe] or over other Fe-peak elements starts to decrease. Additionally, light/odd-Z elements, like Na, Al, Sc, V and Cu, are formed both in Type Ia and II supernovae and are characterized for having an odd atomic number (Z). Finally, elements with $Z > 30$ are the neutron-capture elements and are produced by the capture of neutrons into the nuclei. This process is classified in two types depending on the timescale of the neutron capture. A slow process, longer than the decay of the atom (β decay) is called s-process (Ba, Sr, Y, Zr) and mainly takes place in low and intermediate mass ($< 8M_{\odot}$) AGB stars (Karakas and Lattanzio, 2014; Fishlock et al., 2014), otherwise it is called a rapid process, r-process (Rb, Eu), and likely occur during supernova explosions (Winteler et al., 2012) or mergers of neutron stars (van de Voort et al., 2015; Tanaka et al., 2017; Yong et al., 2021). There still is a lot of discussion about their actual formation site (see Thielemann et al., 2011; Haynes and Kobayashi, 2019)

In addition to chemical abundances, stellar ages are another fundamental parameter to understand the Galactic chemical evolution. Stellar ages allow us to reconstruct the time dimension of Galactic history, therefore, it is of crucial importance to be able to properly determine them in different stellar populations, in order to know the moment in which each evolutionary event occurred, along with its respective duration. Because of this, different techniques have been developed in recent years to determine the ages of stars (see Soderblom, 2010), among which isochrone fitting stands out along with asteroseismology (Kjeldsen and Bedding, 1995; Chaplin and Miglio, 2013; Silva Aguirre et al., 2015), stellar activity (Skumanich, 1972; Pace et al., 2009; Lu et al., 2021) or gyrochronology (e.g. Barnes, 2003, 2007; Godoy Rivera, 2021).

1.1 Chemical clocks

During recent years, several studies have found in FGK low-mass stars that there are some abundance ratios like [Y/Mg], [Y/Al] and [Ba/Mg] that follow a linear relation

with stellar age (da Silva et al., 2012; Nissen, 2015; Feltzing et al., 2017; Titarenko et al., 2019; Delgado Mena et al., 2019). These ratios are derived from [X/Fe] ratios, by

$$[\mathrm{A/B}] = [\mathrm{A/Fe}] - [\mathrm{B/Fe}] \tag{1.1}$$

with their respective uncertainty being

$$\delta[\mathrm{A/B}] = \sqrt{\delta A^2 + \delta B^2} \tag{1.2}$$

So for example, [Y/Mg] = [Y/Fe] − [Mg/Fe]. A way to understand why this happens is explained in Nissen (2015), and it is based on the fact that different nucleosynthesis processes occur over different timescales depending on the masses of the stars.

Given the nature of each nucleosynthetic family, we can observe, for example, that elements that are produced in core-collapse supernovae from massive stars, like α-elements (Nomoto et al., 2013), have a very different production rate compared with those produced in late AGB stages of intermediate mass stars, like s-capture elements (Karakas and Lattanzio, 2014). Because these two processes enrich the ISM over different timescales, we see now a dependence with stellar age when comparing the two families of elements.

Following this idea of different chemical enrichment rates for elements of different nucleosynthetic channels, Jofré et al. (2020) looked for more trends in abundance ratios between different nucleosynthetic families using a large sample of solar twins analyzed by Bedell et al. (2018). They found that 55 different abundance ratios have similar *chemical clock*-behavior. All these ratios involved neutron-capture elements (mostly s-process). These abundances also have shown to add crucial information in chemical evolution studies for metal-poor stars (see Skúladóttir et al., 2019).

Although chemical clocks have been the subject of many studies, their applications and limitations are not yet fully understood, but we know that their calibration relies on very precise determination of stellar ages and abundances. High-precision abundance analysis can be done by performing line-by-line differential analyses using a star with sim-

ilar stellar parameters as reference, like the Sun for solar-twins. This helps to minimize the effects of systematic errors in the derivation of the abundances such as approximations in the model atmospheres and/or inaccuracies in the atomic data, and thus achieve high-precision measurements (see Jofré et al., 2019; Nissen and Gustafsson, 2018, for more details). These levels of precision ($\sim$ 0.01 dex Meléndez et al., 2009) open the door to new ways of multidimensional studies of the chemical evolution of the Milky Way (e.g. using evolutionary trees Jofré et al., 2017a; Jackson et al., 2021). At the same time, precise determination of stellar ages is usually difficult in main-sequence stars where isochrones cannot be easily differentiated, because the theoretical curves have similar evolutionary trajectories and are very close to each other along this sequence. High-resolution spectroscopy and differential stellar parameters are key to mitigate the effects of this problem and estimating ages with uncertainties $\sim$ 1 Gyr (e.g. Nissen et al., 2020).

Feltzing et al. (2017) challenged the chemical clock applicability of [Y/Mg] by showing that it depends on metallicity. Such dependencies have been further studied for [Y/Mg], [Y/Al] by Casali et al. (2020) and [Sr/Mg] by Nissen et al. (2020) showing a significant effect, leading to the conclusion that chemical clocks are not universal and have to be used carefully in attempts of estimating stellar ages. Moreover, Casamiquela et al. (2021b) used a large sample of open clusters with well-known ages, to show that offsets and dispersion are introduced in the age-abundance relations when reaching out of the local bubble ($d > 1$ kpc), showing that studying trends of chemical abundance ratios with age in open clusters is prone to contamination due to radial migration if the sample includes clusters outside the local bubble. This dependency on metallicity and spatial volume are excellent evidence that chemical clocks really carry information about chemical evolution, which might be different at different places in the galaxy. Hence, it is not straightforward to apply these chemical-clock relations outside the solar-metallicity nor solar-vicinity.

1.2 Wide binaries

Another test that could be performed to evaluate the applicability of chemical clocks would be to study how consistent they are between stars that were born together, with

systems that allow covering a much greater range of ages and metallicities than what the population of open clusters can provide.

Wide binaries meet these conditions. These are systems of two stars gravitationally bound to each other, with consistent properties and orbital separations 100AU $< a <$ 1pc, thus they are far enough apart that they cannot interact with each other (i.e. mass transfer) and are assumed to have evolved independently. Their possible formation scenarios, such as the association of pairs of stars during the dissolution of their cluster of stars birth of a single age (Kouwenhoven et al., 2010; Peñarrubia, 2021), dynamic deployment of triple systems (Elliott and Bayo, 2016), turbulent fragmentation (Lee et al., 2017), and gravitational attraction of nearby prestellar nuclei (Tokovinin, 2017), imply that their components are formed in a common origin, being open cluster analogs of only two stars. As a consequence, the components of wide binaries are expected to have similar chemical compositions and ages. To our knowledge, the only one work that studies the coevality of wide binaries with a large sample of systems is that of Kraus and Hillenbrand (2009) where they confirmed that young binary stars in Taurus-Auriaga association are coeval within ~ 0.16 dex in $\log \tau$. Even so, there are other studies of individual systems (Saffe et al., 2017; Reggiani and Meléndez, 2018; Maia et al., 2019; Nissen et al., 2020, e.g.) that have found that the ages of the components of wide binaries are in good agreement, but they are not exempt from presenting some differences, as is the case of Maia et al. (2019), where variations of about 0.7 Gyr in 16 Cygni stars are found, yet remain consistent within the uncertainties. Although these results support the formation scenarios of wide binaries, it is still necessary to demonstrate their coevality using a statistically significant sample.

Several studies have already analyzed chemical abundances in wide binary systems (e.g. Oh et al., 2017; Ramírez et al., 2019; Hawkins et al., 2020; Nelson et al., 2021) and found that they are very homogeneous (within ~ 0.1 dex and ~ 0.05 dex for stars with similar $T_{\rm eff}$). Recently, this was corroborated even for ultra-wide comoving pairs, where Nelson et al. (2021) studied co-moving pairs with separations of five orders of magnitude ($> 2 \times 10^5$ AU) and found that a fraction of $\sim 75\%$ are co-natal based on their metal-

licities. On the other hand, some studies also have found that there are some cases in which the components of wide binaries seem to have statistically significant differences in chemical composition. If the chemical abundances follow a trend with condensation temperature, this can be typically attributed to planetary formation or planet engulfment (Meléndez et al., 2009; Teske et al., 2015; Maia et al., 2019), enhancing the abundances of refractory and/or Fe-peak elements. Hawkins et al. (2020) used a sample of 25 wide binaries such that their components were of similar spectral type and found that odd-z elements, Fe-peak, α-elements, and neutron-capture elements are very consistent, in contrast to what is found for random pairs.

Originally proposed by Andrews et al. (2018, 2019), wide binaries are an ideal sample for studying Galactic chemical tagging (Freeman and Bland-Hawthorn, 2002), because the consistency in the detailed chemistry of their components (e.g. abundances and metallicity) imply a common origin for these stars. In addition, wide binaries span a wider range of age and [Fe/H] than open clusters, thus making it possible to understand the possibility of chemical tagging over a more representative fraction of the Galactic stellar populations.

1.3 Chemical clocks in wide binaries

In this thesis, we aim to evaluate how consistent are the various chemical clocks among the components of wide binary systems, taking advantage of their expected contemporary nature. For this, we used a sample of wide binaries with FGK components spanning a wide range of metallicities and analyzed with high-precision by implementation of a differential analysis, to then compare the consistency of chemical clocks and individual abundances in these systems.

1.4 Structure

We begin by describing the whole sample of wide binaries in Chapter 2 which is comprised by our sample and a compilation from the literature. In Chapter 3 we explain the process with which we derived the stellar parameters and chemical abundances of our sample. Results regarding chemical homogeneity are explained in Chapter 4, and in Chapter 5 we present a detailed analysis of the consistency found in chemical clocks and a small exercise to apply these abundance ratios in chemical tagging. Finally, our conclusions and future work are presented in Chapter 6.

Chapter 2

Sample of wide binaries

2.1 Our sample

For this thesis, we started with a sample of 5 wide binaries with solar-type components which have been previously classified as bonafide binaries using common proper motions and photometry in Chanamé and Gould (2004), and Gould and Chanamé (2004). We checked their parallaxes (ϖ) and radial velocities from *Gaia* EDR3 (Gaia Collaboration et al., 2021), to confirm that the pairs belong to a wide binary system. We also computed the projected separation s of each system

$$s = \theta \times 1/\varpi \tag{2.1}$$

considering the inverse of the mean parallax as distance ($d \sim 1/\varpi$), where θ is the angular separation between two stars, A and B, located nearby in the sky and derived from their right ascension (α) and declination (δ)

$$\theta = \sqrt{(\alpha_A - \alpha_B)^2 \cos\delta_A \cos\delta_B + (\delta_A - \delta_B)^2} \tag{2.2}$$

These five systems were observed between September 2011 and January 2012[1] with the high-resolution Magellan Inamori Kyocera Echelle (MIKE; Bernstein et al., 2003) spectrograph on the 6.5 m Magellan Clay telescope located at Las Campanas Observa-

[1]CN2012A-063 and CN2012A-064 CNTAC programs

Table 2.1: Right ascension (α), declination (δ) (both in J2000), parallax (ϖ) and proper motion (μ) from *Gaia* eDR3, together with observational data, and projected separations of our sample of five wide binaries

Star	α (deg)	δ (deg)	ϖ (mas)	μ_α (mas yr^{-1})	μ_δ mas yr^{-1})	Date (s)	Exp time	S/N (AU)	s
HIP32871	102.75	-56.24	13.32±0.01	-29.53±0.02	46.05±0.01	2011 Sep 09	1711.9	344	1254.51
HIP32865	102.74	-56.24	13.31±0.01	-27.53±0.01	46.57±0.01	2011 Sep 09	2473.9	342	
HIP34426	107.05	15.52	20.97±0.02	-54.21±0.03	-212.84±0.02	2012 Jan 23	2615.4	506	8218.91
HIP34407	107.00	15.53	21.02±0.02	-51.69±0.03	-206.17±0.02	2012 Jan 23	1800.0	409	
HIP52792	161.90	-15.63	12.08±0.13	-113.07±0.11	-45.05±0.14	2011 Nov 04	365.9	332	2594.17
HIP52793	161.90	-15.62	11.56±0.04	-118.40±0.04	-47.48±0.04	2011 Nov 04	1911.8	355	
HIP58240	179.18	-32.27	28.23±0.02	-171.87±0.03	-8.14±0.02	2012 Feb 22	1787.6	299	664.31
HIP58241	179.18	-32.27	28.21±0.02	-179.09±0.03	-6.55±0.02	2012 Feb 22	1440.0	297	
HIP15304	49.36	7.66	21.27±0.02	166.36±0.03	-6.31±0.02	2011 Sep 08	661.5	310	7374.10
HIP15310	49.39	7.69	21.23±0.02	168.81±0.03	-6.39±0.02	2011 Sep 08	792.0	288	
VESTA	318.48	-22.89	-	-	-	2011 Nov 06	360.0	255	

tory. It has a resolution of $R \sim 65,000$ for the red, and $R \sim 85,000$ for the blue orders. The observations were carried using a slit of $0.35'' \times 5.00$ and a binning of 1×1. In addition, we considered a solar spectrum taken from VESTA, also observed in that period. The spectra cover a range of 3380Å to 9370Å and have signal-to-noise (S/N) above 250, which was measured from the fluxes between 777.65 nm and 777.95 nm, because it is a region free from absorption lines. Data reduction was done using the MIKE Carnegie-Python pipeline[2] (Kelson, 2003; Kelson et al., 2000).

Figure 2.1 shows the oxygen triplet of our five wide binaries, where the primary and secondary component are in blue and orange, respectively. Here we see that some components have differences in shape and/or strength of their lines, which besides being caused by abundance differences can be due to line broadening, like the case of HIP 58240/HIP 58241, a system with a young and active pre-MS primary (Chanamé and Ramírez, 2012).

[2] `https://code.obs.carnegiescience.edu/mike`

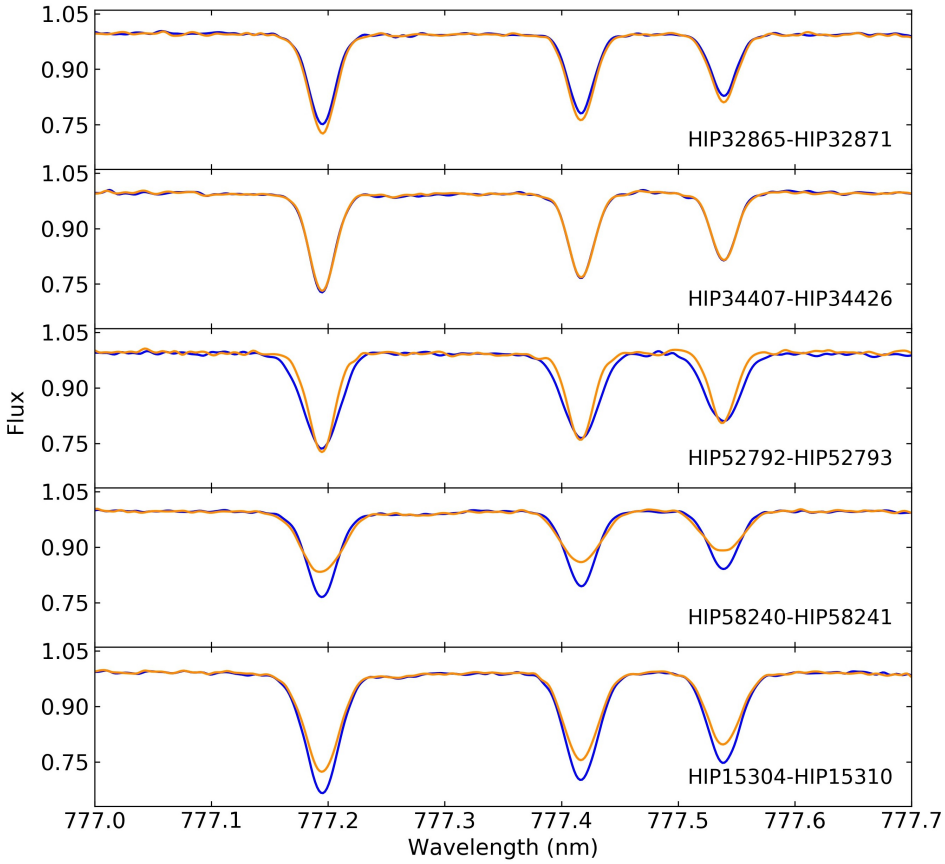

Figure 2.1: One-dimensional spectra of our sample of wide binaries, centered in the oxygen triplet lines at ∼777 nm. The primary component is shown in blue and the secondary in orange.

2.2 Wide binaries in Literature

To improve the statistics of our analysis of chemical clocks, we include 32 wide binary systems for which high-resolution spectral analysis have been performed in the literature, and abundances or equivalent widths (EWs) are available. More information about these systems, like stellar parameters, astrometry and abundances can be found in Table A.1.

For systems HAT-P (Saffe et al., 2017), HD 20782/HD 20781 (Mack et al., 2014), HD 80606/HD 80607 (Liu et al., 2018), WASP-94 (Teske et al., 2016), XO-2 (Ramírez et al., 2015), HD 134439/HD 134440 (Reggiani and Meléndez, 2018), and ζ Ret (Saffe et al., 2016), we used the available EWs published by the authors to derive their abundances using the same methodology than for our own observations (explained in Section 3). In

almost all of these systems, except for the last two, it has been possible to probe that at least one of its components hosts planets. Although the existence of planets in HD 134439/HD 134440 and ζ Ret has not been confirmed, they also present a slight difference in their chemical composition, of about 0.06 dex (Reggiani and Meléndez, 2018) and 0.04 dex (Saffe et al., 2016) in [Fe/H], respectively. This has been interpreted as possible signs of engulfment in HD 134439/HD 134440, and the existence of a debris disk around ζ^2 Ret (Eiroa et al., 2010).

This last system is very peculiar. Nissen et al. (2020) found it is depleted in yttrium compared to other stars of similar ages. In addition to this, their isochrone and activity ages are significantly lower than the chemical ages derived with [Y/Mg] (9.1 ± 0.5 Gyr for ζ^1 Ret and 9.4 ± 0.5 Gyr for ζ^2 Ret), which implies that its atmosphere behaves like that of a young star, despite being chemically and kinetically old. A plausible explanation for this if that they are blue straggler stars formed by short period binaries (Rocha-Pinto et al., 2002).

The abundances of the remaining 25 wide binaries were taken from Hawkins et al. (2020, hereafter H20), where they derived parameters and abundances with spectral synthesis using the BACCHUS code (Masseron et al., 2016). We noted that their system called WB01 is in fact HD 80606/HD 80607 (Liu et al., 2018). In order to avoid counting it twice, we only kept its data from H20.

There are no studies that confirm or refute the existence of planets in our systems or those of H20 (except for WB01 and HIP 34426/HIP 34407). Despite this, in H20 they mention that the condensation temperature trend of the 5 systems with Δ[Fe/H] > 0.1dex was studied and that, in some cases, there is indeed a clear correlation indicating accretion of rocky material, but they do not go further into the subject. The advantage of including some binary systems whose components present variations in their chemical patterns, is that it will allow us to test the consistency of chemical clocks even when there have been additional factors that could alter the chemical composition of the stars, such as primordial differences (i.e. planet formation and engulfment) or stellar evolution.

The top panel of Figure 2.2 shows our entire sample of stars in *Gaia* EDR3 color-magnitude diagram (CMD) divided into 3 groups: our five wide binaries (green), H20 systems (orange), and the rest of the systems from literature (blue). For reference we show in grey circles the catalog of wide binaries from El-Badry and Rix (2018). The bottom panel shows a Kiel diagram ($T_{\rm eff}$ vs $\log g$) colored by metallicity, where the dashed lines point the location of the Sun. Each binary is connected with a black line, which allows us to see that the components have very similar colors, absolute magnitudes and stellar parameters.

Most of the pairs are well placed in the expected main sequence locus, except for HD 134439/HD 134440, which is located below. The components of this binary are very metal-poor (-1.43 dex and -1.39 dex, respectively), so they are much less affected by blanketing, and therefore, bluer than a star with the same mass but higher metallicity (i.e. solar). In Reggiani and Meléndez (2018) they found that its chemical composition and kinematics are not consistent with low-α nor high-α halo stars, but instead suggest that it might have formed in a dwarf galaxy similar to Fornax. This possible intergalactic origin makes it an interesting object to test chemical clocks.

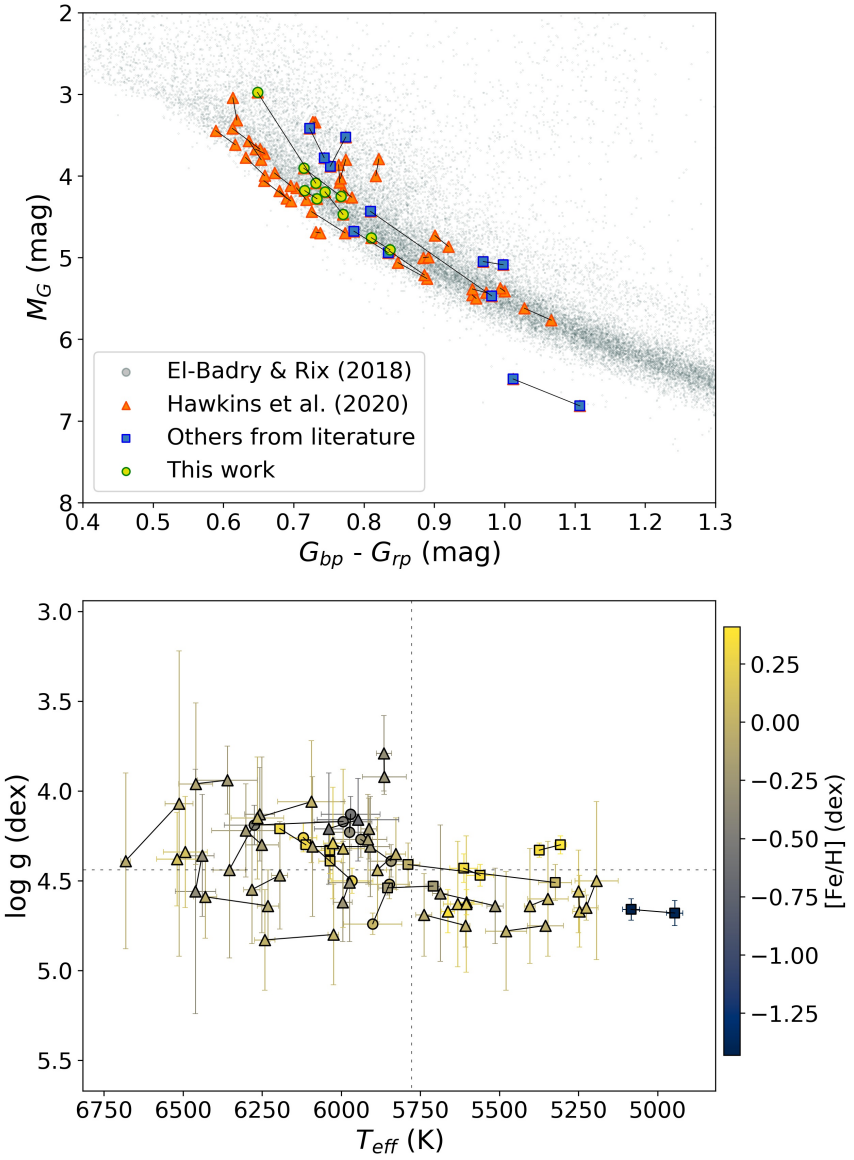

Figure 2.2: Top: *Gaia* DR3 color-magnitude diagram of the stars used in this work. Background stars (grey) were taken from El-Badry and Rix (2018) catalog of wide binaries. Bottom: Kiel diagram ($T_{\rm eff}$ vs $\log g$) colored by metallicity. The dashed lines show the position of the Sun. HD 134439/HD 13440 is separated from the rest of the sample and lies below the main sequence, given that it is very metal-poor and suffers much less blanketing in comparison with other more metal-rich stars of the same mass.

Chapter 3

Spectroscopic analysis

3.1 Spectroscopy with iSpec

The spectral analysis was done using the spectroscopic framework `iSpec` (Blanco-Cuaresma et al., 2014; Blanco-Cuaresma, 2019), a Python wrapper capable to run several state-of-the-art radiative transfer codes and model atmospheres. It implements several functions for basic spectra manipulation (e.g. S/N estimation, telluric determination, continuum normalization), along with functions to compute radial velocities, atmospheric parameters, and individual chemical abundances.

3.1.1 Data preparation

For each spectral order its continuum was fitted by applying a median-maximum filter to the fluxes to reduce the effects of noise and ignore the deeper fluxes of absorption lines. Then, it was modeled with a third-degree spline function every 5 nm ignoring prefixed strong lines like tellurics and strong absorption lines identified and masked using a telluric line list from iSpec. After normalization, the orders were stacked using `scombine` task from IRAF using the median value of the fluxes.

The one-dimensional spectra were corrected by their barycentric velocities with iSpec before determining the radial velocities from cross-correlation with a solar spectrum from NARVAL ($370 - 1048$ nm) provided by this framework.

3.1.2 Stellar parameters

Both abundances and stellar parameters were determined from the observed EW, which were measured with iSpec fitting a Gaussian profile to each line. For the abundance determination, we selected the lines whose strength falls mainly in the linear part of the curve of growth (Gray, 2008), to avoid saturated or very weak lines. In all our procedure we used Local Thermodynamic Equilibrium (LTE) MOOG[1] radiative transfer code (Sneden, 1973; Sneden et al., 2012, 2017 version) and MARCS[2] 1D models (Gustafsson et al., 2008) because they ensures a more realistic temperature structure of the model atmospheres (Blanco-Cuaresma, 2019)

The stellar atmospheric parameters were determined with iSpec using the classic spectroscopic method: excitation-ionization balance. This method requires no correlation between excitation potential and iron abundance derived from several absorption lines, that is, imposes excitation balance. In addition, it requires having same abundances derived from neutral and ionized iron lines, known as ionization balance. That way it is possible to constrain the effective temperature $T_{\rm eff}$ and surface gravity $\log g$, respectively. Finally, microturbulence velocity $v_{\rm mic}$ is obtained imposing a flat slope in the iron abundance as a function of the reduced equivalent width (REW) of each line. The errors on the stellar parameters were automatically calculated with iSpec, from the co-variance matrix constructed by the nonlinear least-squares fitting algorithm (Blanco-Cuaresma et al., 2014).

We used the extended selection of lines provided by iSpec that covers a range of $480\,\mathrm{nm} - 615\,\mathrm{nm}$ with 154 neutral and 11 singly-ionized iron lines. Atomic data were taken from the fifth version of the linelist of atomic data from Gaia-ESO Survey (GES) (Heiter et al., 2021) and we considered the solar abundance from Grevesse et al. (2007). Finally, we discarded outlier lines using a robust regression of 0.9 with iSpec, to prevent any strong dispersion in the data. Our resulting stellar parameters are listed in Table 3.1.

[1] `http://www.as.utexas.edu/~chris/moog.html`
[2] `https://marcs.astro.uu.se/`

Table 3.1: Radial velocity, effective temperature, surface gravity, metallicity, and microturbulence velocity of our sample of five wide binaries obtained with iSpec

Star	RV (km s^{-1})	$T_{\rm eff}$ (K)	$\log g$ (dex)	[M/H] (dex)	$v_{\rm mic}$ (km s^{-1})
HIP32871	0.25±0.26	5938 ± 82	4.27 ± 0.10	-0.24 ± 0.01	1.21 ± 0.04
HIP32865	0.0±0.24	5843 ± 72	4.39 ± 0.09	-0.23 ± 0.01	1.01 ± 0.04
HIP34426	-12.15±0.28	5970 ± 93	4.13 ± 0.10	-0.55 ± 0.01	1.26 ± 0.06
HIP34407	-12.64±0.24	5974 ± 73	4.23 ± 0.10	-0.34 ± 0.01	1.26 ± 0.04
HIP52792	29.63±0.42	6275 ± 94	4.19 ± 0.11	-0.43 ± 0.02	2.03 ± 0.05
HIP52793	28.99±0.28	5994 ± 91	4.17 ± 0.11	-0.47 ± 0.02	1.33 ± 0.04
HIP58240	6.21±0.22	5848 ± 65	4.52 ± 0.08	-0.01 ± 0.02	1.41 ± 0.04
HIP58241	7.0±0.32	5901 ± 92	4.74 ± 0.06	0.03 ± 0.02	2.00 ± 0.08
HIP15304	31.54±0.24	6120 ± 42	4.26 ± 0.08	0.22 ± 0.09	1.62 ± 0.08
HIP15310	32.18±0.24	5966 ± 66	4.50 ± 0.07	0.25 ± 0.08	1.35 ± 0.03
VESTA	-5.26±0.2	5799 ± 66	4.49 ± 0.09	-0.01 ± 0.07	1.07 ± 0.04

The system HIP 34426/HIP 34407 is the only one of our sample that has been spectroscopically analyzed in the literature. Ramírez et al. (2019) determined their stellar parameters using a differential approach with the $q2$ code[3] and obtained $T_{\rm eff} = 5925 \pm 12$ K, $\log g = 4.33 \pm 0.03$ dex and [Fe/H] = -0.367 ± 0.010 dex for HIP 34407, and $T_{\rm eff} = 6007 \pm 8$ K, $\log g = 4.32 \pm 0.02$ dex and [Fe/H] = -0.544 ± 0.006 dex for HIP 34426. These values are in good agreement with our results within the uncertainties. Also, they estimated that their ages are 6.5 ± 0.8 Gyr and 6.6 ± 0.8 Gyr, respectively, assuming that both stars have identical internal metallicities of about -0.28 dex.

3.1.3 Chemical abundances

Chemical abundances were determined from EWs using an extended selection of lines from different chemical species provided by iSpec. This list is adapted for the model atmospheres, radiative transfer code and linelist we use (see Section 3.1.2).

[3]The Qoyllur-Quipu (q2) code(Ramírez et al., 2014) `https://github.com/astroChasqui/q2`

The linelist and the radiative transfer code include a treatment for hyperfine structure splitting (HFS) for Sc I, V I Mn I, Co I, Cu I, Ba II, Eu II, La II, Pr II, Nd II, Sm II. Also, it considers isotopic shifts for Zr I and Nd II. That way we measured abundances of 23 different elements from the following nucleosynthetic families: carbon, α (O, Mg, Si, Ca, Ti), neutron-capture (Sr, Y, Zr, Ba, La, Ce), odd-Z (Na, Al, Sc, V, Cu), and iron-peak elements(Cr, Mn, Fe, Co, Ni, Zn). We use the same nucleosynthetic classification as in Jofré et al. (2020). Carbon abundances were determined using C I lines. Oxygen abundances were determined using the oxygen triplet at 777 nm, and corrected by non-LTE effects with values extracted from MPIA (M. Kovalev et al., 2018)[4]. These corrections typically ranged between -0.64 and -0.9 dex, with variations smaller than 0.1 dex within the components of each system (see Table A.3).

Once individual line absolute abundances are measured, strictly line-by-line differential abundances can be computed. For the element X, the differential abundance ΔX is defined as the mean value of the difference in abundance of each line with respect to the same lines in the reference star:

$$\Delta X = \frac{1}{N}\sum_{i=1}^{N}(A_{X,i} - A_{X,\mathrm{ref}}) \tag{3.1}$$

Where $A_{X,i}$ is the absolute abundance of the ith-line of the given star, $A_{X,\mathrm{ref}}$ is the absolute abundance of the same line measured in the reference star, and N is the number of lines. Here, the reference star is the Sun, whose abundances are obtained from the spectrum of VESTA.

Uncertainties in element abundances were obtained using the standard error (SE = $\sigma/\sqrt{N}$) when more than three lines were available. This error estimation method is frequently used (e.g. Meléndez et al., 2012; Ramírez et al., 2015; Adibekyan et al., 2016), but it is important to recall that in the case of elements with few lines it can underestimate the real dispersion, and it is recommended to use the median with the interquartile ($q_{75} - q_{25}$) range as its uncertainty, because it is a more robust estimator of the abun-

[4]http://nlte.mpia.de

dances (see Jofré et al., 2018).

For elements with only one spectral line available we used a conservative error of 0.03, which is the maximum error for the elements with more than 3 lines. Also, we take into account the effects of the uncertainties in stellar parameters by computing the sensitivity $\sigma_{\rm sens}$ for each element. Following Casamiquela et al. (2020) this $\sigma_{\rm sens}$ is the dispersion in abundances obtained when varying the stellar parameters by their uncertainties. The final uncertainty is obtained by adding in quadrature the element sensitivity and the standard error

$$\sigma_{tot} = \sqrt{\mathrm{SE}^2 + \sigma^2_{\rm sens}} \tag{3.2}$$

3.2 Abundances of wide binaries from the literature

The abundances of systems collected from the literature (except H20) were determined from their EW list using the stellar parameters reported by the authors (which were derived differentially from excitation-ionization balance), and following a similar method as ours (Section 3.1.3). In addition, the authors of the analyses of the seven systems taken from the literature reported the EWs of the reference star that they used (usually VESTA, except for HD 134439/HD 134440 where they used HD 103095). We used this information to perform the differential analysis in the same way as for our systems. Something important to recall is that each of these systems was observed within a different spectral range, therefore their abundances were determined with different lists of lines. Also, we placed the abundances of the H20 sample to Grevesse et al. (2007) scale for consistency.

Our final sample of wide binaries consists of 36 systems (72 stars) with stellar parameters that span a range of $\sim 4946 - 6682$ K in $T_{\rm eff}$, $\sim 3.79 - 4.83$ dex in $\log g$ and $\sim -1.43 - 0.41$ dex in [Fe/H].

Chapter 4

Chemical homogeneity of wide binaries

4.1 Chemical homogeneity in our systems

The chemical homogeneity of stars in wide binaries has been previously studied (e.g. Andrews et al., 2018; Hawkins et al., 2020), showing that these systems generally exhibit very similar chemical patterns within their components, supporting evidence that they are co-natal. The abundance differences ΔX between the components of each of our systems (component A minus component B) are shown in Figure 4.1. In order to help to visualize the precision of the measurements, differential abundances with uncertainties greater than 0.05 dex are colored in gray, whereas orange points depict differences with smaller uncertainties. Each panel also includes the difference in $T_{\rm eff}$, $\log g$ and [Fe/H] between the binary components.

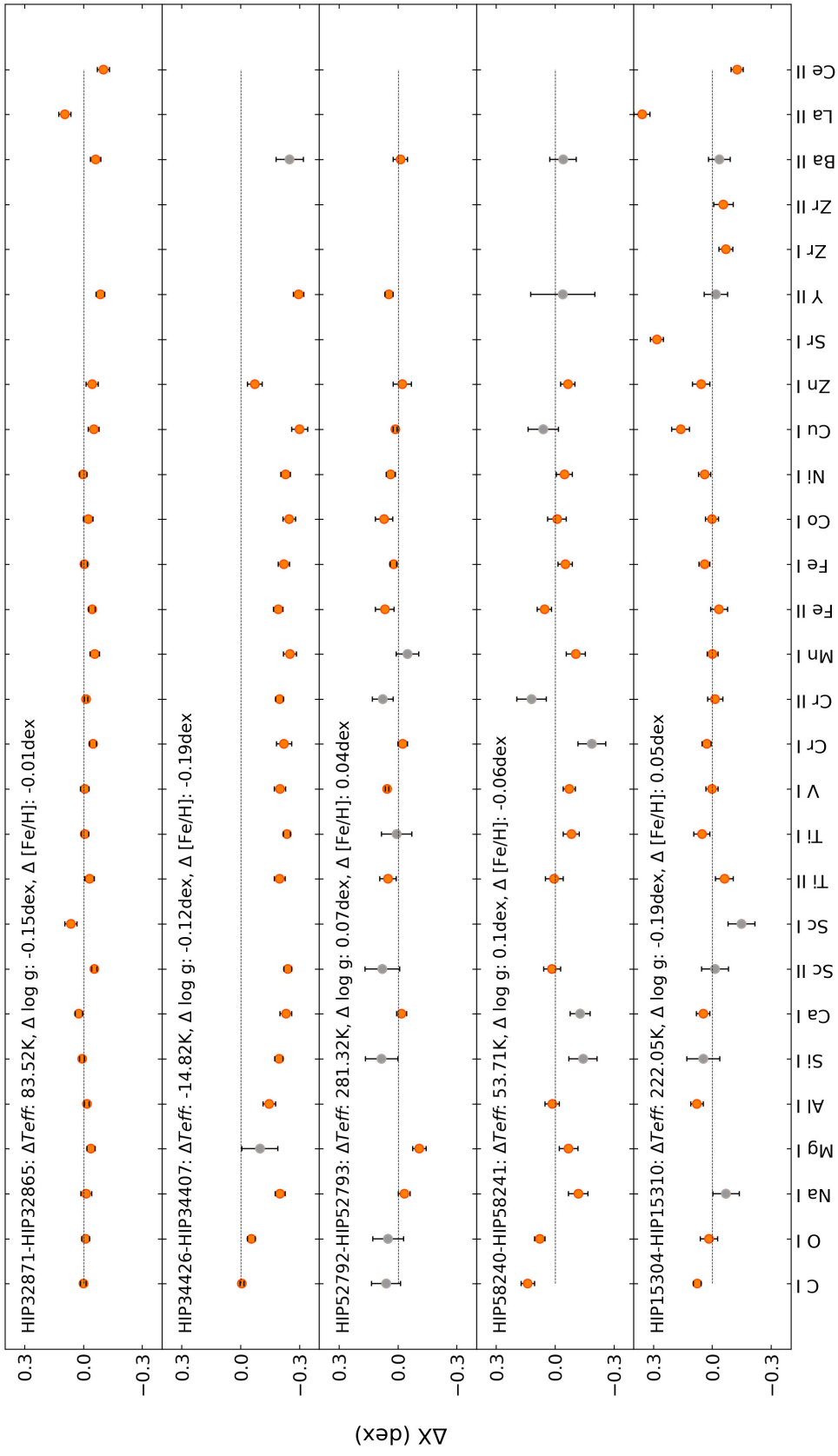

Figure 4.1: Differential chemical abundances of wide binary pairs with solar-twin components. Each panel includes their difference in $T_{\rm eff}$, $\log g$ and [Fe/H]. Grey points are abundances with uncertainties larger than 0.05 dex, whereas orange points depict uncertainties smaller than 0.05 dex. HIP 32871/HIP 32865 is a remarkable case of homogeneity, while HIP 34426/HIP 34407 has large abundance differences of 0.2 dex in average.

In some cases we were not able to measure all the elements listed in Figure 4.1 because the same spectral line was not correctly measured in one or both components of that system. Specifically, this is the case of Zr, Sr I, Sc I, La II and Ce II, most of them neutron-capture elements which are known to be hard to measure since their lines are weak and sometimes blended (Jofré et al., 2019). In general, ΔX is very close to zero (on average ~ 0.1 dex), bearing out that wide binary systems are indeed chemically homogeneous, in agreement with previous results found in the literature.

HIP 32871/HIP 32865 differential abundances are on average of about ~ 0.06 dex, being a remarkable case of homogeneity whereas HIP 34426/HIP 34407 has average abundance differences of ~ 0.2 dex in most of the elements, being the most inhomogeneous system in our sample and being comparable to Kronos and Krios (Oh et al., 2018), a wide binary enhanced in refractories by ~ 0.2 dex. HIP 34426/HIP 34407 was also studied in Ramírez et al. (2019), where they proposed and analyzed several scenarios that could be causing this difference in their chemical composition: (i) perhaps they are not binary from birth, (ii) engulfment of planetary material rich in refractories, and (iii) inhomogeneities in the gas cloud where they were formed. Despite the efforts, it has not yet been possible to confirm which of these scenarios led to this peculiar system. RV follow up suggests the presence of a Jupiter-like planet or a third star in the system around HIP 34426, while its T_c trend suggests the engulfment of a rocky planet. They also looked for evidence of circumstellar material given the similarity of the T_c trend with that of RV Tau stars, but found nothing. Then they studied the effects of diffusion, but discarded it because both stars have very similar $\log g$ and unlikely different turbulence.

Regarding how consistent wide binaries are in the different nucleosynthetic families, we find that the mean ΔX (excluding HIP 34426/HIP 34407) are $\sim$0.02 dex for neutron-capture (Sr, Y, Zr, Ba, La, Ce), $\sim$0.003 dex for α (O, Mg, Si, Ca, Ti), $\sim$0.03 dex for odd-Z (Na, Al, Sc, V, Cu), and $\sim$0.03 dex for Fe-peak elements (Cr, Mn, Fe, Co, Ni, Zn). This is in good agreement with Hawkins et al. (2020).

4.2 Chemical homogeneity of the whole sample

Figure 4.2 shows a comparison of the [X/Fe] for the 24 chemical species, for the full dataset of wide binaries. The full sample analyzed in this paper is depicted as follows: our wide binaries (green), H20 (orange) and the rest of the systems from the literature (blue). Each panel shows a different element, which is indicated at its bottom right. [Fe/H] is included in the bottom right panel. The abundances are compared considering one component in the X axis and one component in Y axis, expecting to follow a 1-1 line if the abundances were to match exactly.

In order to quantitatively study the degree of homogeneity of the abundances in wide binaries we compare them with the chemical behavior of random pairs, which are not expected to follow the 1-1 line as wide binaries, given that their components were not formed together. We constructed random pairs selecting stars according to their position in the CMD (Figure. 2.2) as follows. We set a star as a reference and choose the two stars (which are not its true companion) closest to it in the diagram. This is done because our sample has stars that were analyzed with different lists of lines, so it is very likely that by only selecting the closest star, there will not be an absolute match between the lines of the components of the random systems. This could considerably reduce the number of these systems in each [X/Fe] and affect our statistics. This exercise is done for each of the 72 stars of the whole sample, creating a total of 144 random systems. Grey contours show the distribution of the random pairs if at least three of them have measurements of that [X/Fe]. We note H20 does not have abundances of O or Ce. That is why some of these panels, in addition to lacking orange points, lack gray contours.

In Figure 4.2 we can see that wide binaries are generally more tightly distributed along the 1-1 line than random pairs, as expected from previous works (Desidera et al., 2006; Andrews et al., 2018). In general, almost all of the elements show solar abundance patterns and follow a similar distribution centered at zero, possibly because these stars belong to the solar neighborhood. Exceptions to this are Ba II, Mn I, Cu I, La II and Co I, which span a wider range in [X/Fe], reaching values above 0.5 dex. Regarding random pairs, they also tend to be concentrated within this range, except in some cases

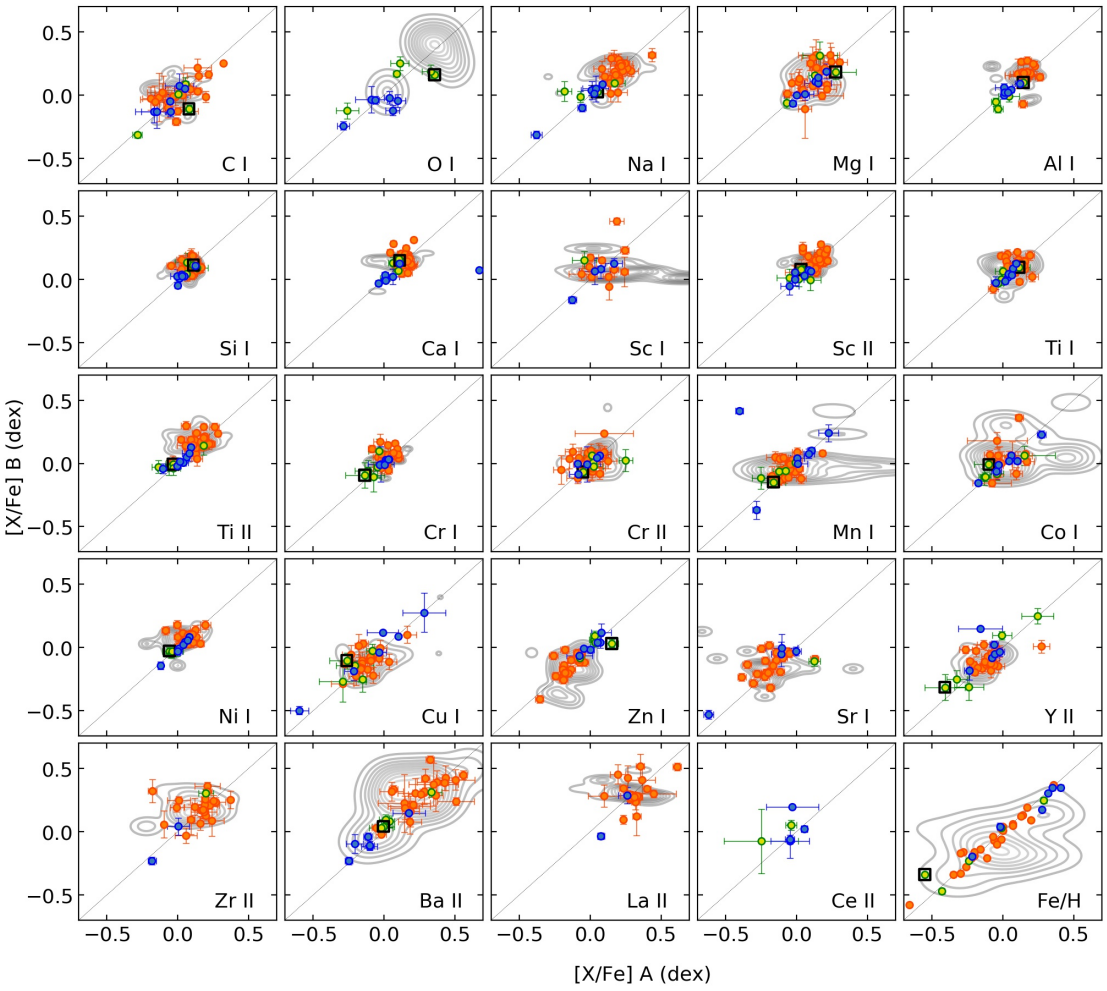

Figure 4.2: Comparison of the [X/Fe] ratios of the two components of wide binaries for all the elements measured in this work. [Fe/H] is in a separated panel at the bottom right of the figure. The systems are colored as: binaries in our sample (green), H20 (orange) and other binaries from literature (blue). The distribution of random pairs is shown as gray contour lines. If there are less than 3 random pairs with [X/Fe], their distribution is not shown. HIP 34426/HIP 34407, the most inhomogeneous system of our sample, is marked with a black square.

(Mn I, Sc I, etc). We further see that some elements show systematic differences among the three samples in the sense that they seem to cover different abundance regimes, e.g. Mn I, Sc I, Ba II, Co I. The reason behind this might be some NLTE effects or the fact that each of these groups were analyzed in different ways (see Section 2.2), using different linelists. Different methodologies, even when using the same prescription and input data, can lead to systematic differences in abundances. In this case, the fact that H20 abundances were determined with spectral synthesis, while EWs were implemented in the rest of the sample can lead to inconsistencies given the different HFS treatment of each method, as discussed in Section 5.3. An extensive discussion on this subject can be found in Jofré et al. (2017b).

According to the excitation-ionization balance, neutral and ionized abundances of an element should be equal, but in practice this is not always the case given NLTE, 3D effects or HFS (see Jofré et al., 2015). We have 3 elements with abundances for the neutral and ionized species: Sc, Cr, Ti. Previous studies have found that Sc I and Cr I are strongly affected by NLTE (Zhang et al., 2008; Bergemann and Cescutti, 2010; Battistini and Bensby, 2015), while for Ti I the corrections are minor, but it is still more sensitive to NLTE (Bodaghee et al., 2003). It is for this reason that we decided to only use the Sc II, Cr II and Ti II measurements as the abundances of each element for the rest of the following analysis.

It's important to mention that our results for elements like Na, Al, Mn, Co and Ba may be slightly affected by NLTE effects, but since we are performing a differential analysis these are minor corrections, these should mostly be represented as translations along the 1-1, not as variations in the dispersion around it. Regarding 3D effects, given that their implementation provides absolute abundances with greater precision (e.g. Nissen and Gustafsson, 2018), it is absolutely necessary to include them when calibrating chemical clocks, but in the case of this work where we only compare the clocks of stars with similar stellar parameters it is not expected that it plays a big role, since the effect of the 3D models on the abundances should be very similar (if not the same) for both.

4.3 Condensation temperature trend

The formation of planets can leave a subtle imprint in their host's stellar atmosphere ($\sim$ 0.01 dex) (Chambers, 2010). While in general planets are formed from the same material as their host star, rocky planets in particular would preferentially remove refractory content (higher T_c), so they may leave the stars slightly poor in these elements (Meléndez et al., 2009; Ramírez et al., 2009; Nissen, 2015). Another scenario in which the stellar composition can be altered are planet engulfment or accretion of material with planet-like composition (e.g. Saffe et al., 2017; Maia et al., 2019), thus given the nature of these cases and following the same logic as before, they should also leave evidence in the abundance of refractory elements of the star.

Figure 4.3 shows Δ[X/H] as a function of condensation temperature, T_c (Lodders, 2003), for H20 and the wide binaries in our sample that present a trend with an absolute value of the slope greater that 3×10^{-5} dex K^{-1} with a significance greater than 2σ. This cut is based on the slopes that have been reported in the literature, with which a trend has been confirmed or denied (Mack et al., 2014; Saffe et al., 2016; Teske et al., 2016; Liu et al., 2018; Reggiani and Meléndez, 2018).

The linear regression was calculated using the function `linregress` of SciPy library[1]. Since this function does not include the individual error of the elements to derive the uncertainty of the fit, nor does it allow to make a weighted fit as suggested in Adibekyan et al. (2016), we performed the linear regression for the abundances with errors smaller than 0.05 dex (orange points in Figure 4.3). The linear regression that better fits the data is plotted as a blue line, and its parameters are included in each panel. We leave the other sample of systems taken from literature (blue systems in Fig. 2.2) out of this plot, because the presence or absence of trend has already been studied in their respective works, and we found their slopes to be consistent with previous results.

In H20 they briefly discussed about this trend in the systems with Δ[Fe/H] $\geq$ 0.1dex, which we identify as WB02, WB05, WB09, WB16 and WB21. Here, we find that three

[1] `https://docs.scipy.org/doc/scipy/reference/generated/scipy.stats.linregress.html`

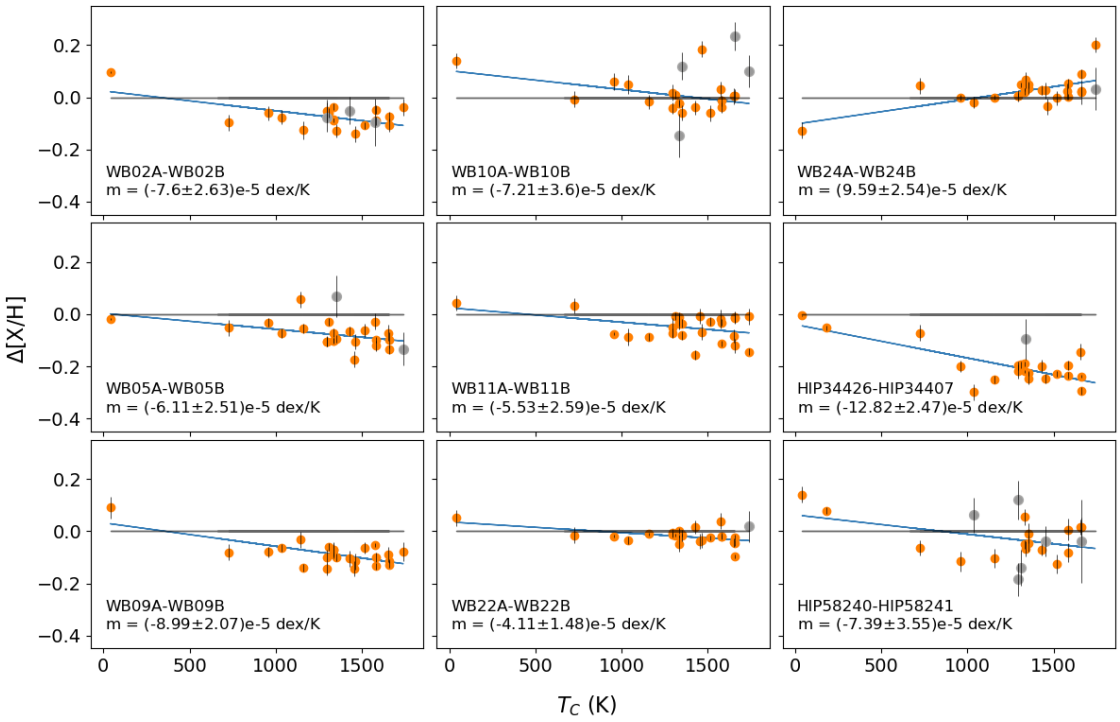

Figure 4.3: Differential abundance as a function of elemental condensation temperature from the H20 systems and our sample of wide binaries that present a slope greater than 3×10^{-5} dex K^{-1}. The blue line shows the linear regression that better fits the data, which parameters are included in the legend of each system. Differential abundances are colored in the same way as in Figure 4.1. The list of elements sorted by increasing T_c is the following: C, O, S, Zn, Na, Cu, Mn, Cr, Si, Fe, Mg, Co, Ni, Ba, Sr, Ce, Ca, La, Ti, Al, Sc, Y, and Zr.

of them, WB02, WB05, and WB21, present a considerable trend, but also WB10, WB11, WB22 and WB24. Regarding our sample, we find that HIP 34426/HIP 34407 and HIP 58240/HIP 58241 also show an important trend with condensation temperature. Ramírez et al. (2019) studied this trend in HIP 34426/HIP 34407 and found a similar behavior. The particular chemical inhomogeneity of this system causes it to have the highest slope among all the wide binaries in this study, for which one would point to the formation or accretion of rocky planets as the main responsible for their nature (as discussed in Ramírez et al., 2019). Something similar could be proposed for the other systems. Despite this, there is still no way to know with certainty which specific mechanism is causing this correlation between chemical difference and T_c just with the information that we handle. Probably, a systematic search for planets in this system would help understanding if the slope is related to this effect.

We noted that the element with the lowest T_c, carbon, seems to have a large influence on the linear regression, so we performed the fit without this element and found that only WB05 and HIP 34426/HIP 34407 keep presenting a significant trend. C I lines have negligible NLTE corrections in solar-type stars (i.e. Caffau et al., 2010), but only a few of them are useful to determine carbon abundances, thus molecular features are implemented. However, it is important to implement 3D atmospheric models in order to have better agreement between atomic and molecular features, as shown in Asplund et al. (2005).

The results presented in this chapter regarding the similar chemical composition of wide binaries (within 0.1 dex) and those found in previous studies, serve as sufficient evidence regarding that these systems are excellent laboratories for chemical tagging, studying effects such as planet presence, and also to test the consistency of chemical clocks. They support the premise that these stars were born together, along with the advantage of them spanning a wide range in metallicity. Furthermore, some of them present differential abundances with a statistically significant trend with T_c and are going to be useful to study the implications of planetary imprints on stellar atmospheres (formation and/or engulfment) on chemical clocks.

Chapter 5

Chemical clocks in wide binaries

In addition to common chemistry that we have evidenced in the previous chapter, the expected common origins of the components of wide binaries imply that they should have similar ages as well (e.g. Kraus and Hillenbrand, 2009). This coevality allows us to test the reliability of the abundance ratios known as chemical clocks (Section 1.1)

We follow Jofré et al. (2020), who used a sample of solar twins to present a large number of combinations of chemical abundance ratios shown to have strong dependency with ages. These relations can be explained with similar arguments as [Y/Mg], which is widely discussed in the literature (e.g. Nissen, 2015; Delgado Mena et al., 2019; Casamiquela et al., 2021b). The argument is the very different timescales for the production of an α-capture element such as Mg in comparison with a neutron-capture element such as Y. When combined, a tight relation of [Y/Mg] with stellar age can be found for stars of the same metallicity. Jofré et al. (2020) and Casamiquela et al. (2021b) found that the clocks showing largest age dependency involved neutron-capture elements with elements produced by other nucleosynthesis channels, as expected given their production scenarios.

We recovered 42 of the abundance ratios using Eq. 1.1 and their respective errors (Eq. 1.2). Figure 5.1 is similar to Figure 4.2 but we plot chemical clocks instead of [X/Fe] abundance ratios. In each axis we plot each component of the binary, expecting the values to follow a 1-1 line given the co-natal nature of the systems. Furthermore, we

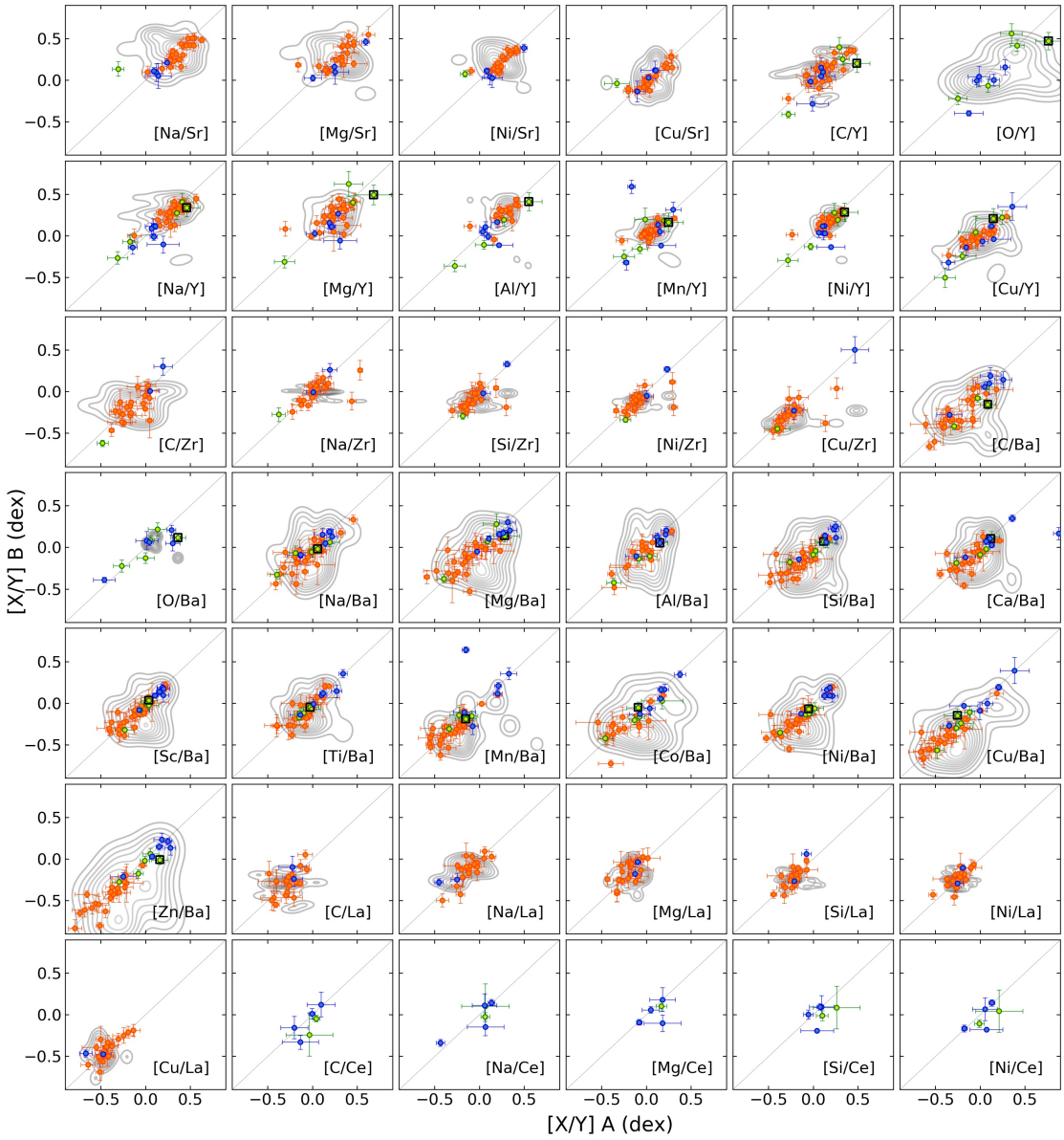

Figure 5.1: Comparison between the components of wide binaries for 42 potential chemical clocks considered in this work. The different systems are colored like in Figure 4.2 and the distribution of random pairs is shown in gray curves. Same as in Figure 4.2, HIP 34426/HIP 34407 is marked with a black square for easy visual identification. The ages related to chemical clocks increase from left to right, so that older stars have more positive values and younger stars more negative values

.

included the distribution of random pairs, like in Figure 4.2. Since H20 lacks Ce and O abundances, there are 8 chemical clocks for which we are unable to have an estimate of a random pair correlation.

In addition, we highlight the system HIP 34426/HIP 34407, which is the least homogeneous wide binary of our sample (see individual results in second panel of Figure 4.1). This system is marked with a black square, and despite being really inhomogeneous this does not seem to have an effect on some of its chemical clocks, especially those that depend on Ba (e.g. [Ti/Ba], [Al/Ba], [Ni/Ba]). Some chemical clocks span a wider range in abundance ratio than others, like [Cu/Ba], [Zn/Ba], [Na/Sr], and [O/Y], particularly because of the H20 sample. As well as in Figure 4.2, we believe that this is mostly due to a systematic effect in the derived abundances, as mentioned in Section 5.3.

5.1 Consistency of chemical ages in wide binaries

In order to quantify the degree of correlation in our data, or lack thereof, we compute the Spearman correlation coefficient (SCC) [1], which measures the linear correlation between two data sets and was chosen given that the chemical clocks and [X/Fe] in this work not necessarily follow a normalized distribution. Each SCC and their respective p-values are presented in Table 5.1 and Table 5.2 for both wide binaries and random pairs. In Figure 5.2 we plot the distributions of the SCC from Figures 4.2 and 5.1, showing wide binaries in orange and random pairs in blue. The coefficients were derived only from those chemical clocks and [X/Fe] ratios with at least 10 random pairs, to ensure robust statistics. Table 5.3 presents the median and median absolute deviation (MAD) of the SCC of chemical clocks and [X/Fe] in wide binaries and random pairs, for better understanding of Figure 5.2.

The top panel of Figure 5.2 shows that standard [X/Fe] abundances are more consistent in wide binaries than random pairs, but the differences between distributions are not

[1] Derived with SciPy: `https://scipy.org`

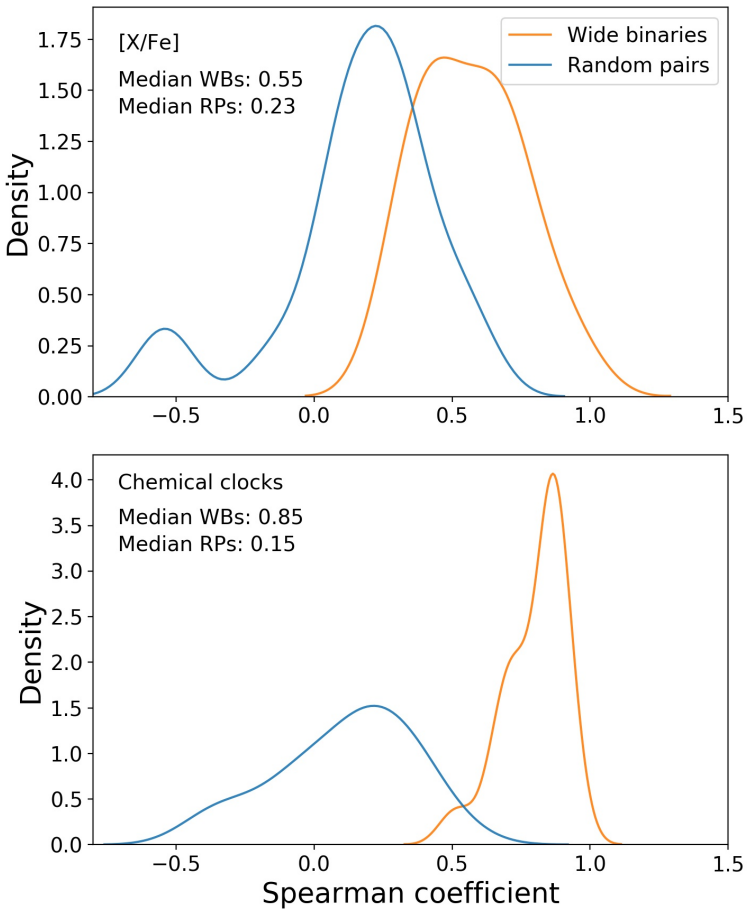

Figure 5.2: Distribution of the Spearman correlation coefficient (SCC) from Figures 4.2 (top) and 5.1 (bottom), implementing a Kernel Density Estimate (KDE) plot smoothed with a Gaussian and colored in orange for wide binaries and in blue for random pairs. Statistical features of each plot are listed in Table 5.3.

so stark. On the other hand, in the bottom panel we can see that the SCC distributions of chemical clocks are very different from each other, since random pairs show a peak at ~ 0.1 while in wide binaries this is at ~ 0.8 (see Table 5.3). Moreover, the areas covered by each distribution almost do not overlap, which means that there is a very low chance that stars that do not necessarily have a common origin can have the same chemical clocks, thus age.

If chemical clocks were just reflecting abundance ratios, their 1-1 correlation should be comparable to the correlation found for other abundances between coeval stars that were born together. However, our results imply that chemical clocks are even more con-

Table 5.1: Spearman correlation coefficients (SCC) and p-values for each individual abundance and [Fe/H] in wide binaries and random pairs, plotted in Figure 4.2

[X/Fe]	SCC	p-value	Random	p-value	[X/Fe]	SCC	p-value	Random	p-value
Fe/H	0.97	4.4e-24	0.26	0.12	Ni I	0.50	1.6e-03	0.37	0.02
Ba II	0.86	1.9e-11	0.61	0.00	Mn I	0.45	4.9e-03	0.39	0.03
Zn I	0.83	2.5e-09	0.34	0.05	Zr II	0.45	2.3e-02	0.23	0.33
Na I	0.74	1.6e-07	0.49	0.00	Cr I	0.42	1.0e-02	0.32	0.05
Ti II	0.71	1.1e-06	0.26	0.13	Si I	0.42	9.2e-03	0.12	0.48
C I	0.71	2.3e-06	0.06	0.73	Ca I	0.37	2.5e-02	0.29	0.09
Al I	0.68	9.7e-05	-0.03	0.88	Ti I	0.37	2.6e-02	0.11	0.51
Cu I	0.67	9.3e-06	0.52	0.00	Cr II	0.35	3.7e-02	0.20	0.28
Sc II	0.66	7.4e-06	0.10	0.57	La II	0.29	1.9e-01	-0.51	0.03
Co I	0.64	2.8e-04	0.09	0.71	Sc I	0.29	2.7e-01	-0.57	0.09
Sr I	0.58	1.8e-03	-0.16	0.47	Ce II	-	-	-	-
Y II	0.55	4.5e-04	0.24	0.18	O I	-	-	-	-
Mg I	0.53	9.9e-04	0.15	0.39					

Table 5.2: SCC and p-values for each chemical clock in wide binaries and random pairs, plotted in Figure 5.1

Clock	SCC	p-value	Random	p-value	Clock	SCC	p-value	Random	p-value
[Zn/Ba]	0.95	8.4e-18	0.41	0.02	[C/Y]	0.81	1.6e-08	0.40	0.02
[Cu/Ba]	0.93	6.2e-16	0.54	0.00	[Si/Zr]	0.76	1.1e-05	0.17	0.46
[Sc/Ba]	0.93	9.5e-17	0.19	0.26	[Na/La]	0.75	5.5e-05	0.43	0.09
[Ni/Ba]	0.90	9.5e-14	0.30	0.08	[Na/Zr]	0.74	2.2e-05	-0.36	0.12
[Na/Sr]	0.89	7.1e-10	-0.05	0.81	[Ni/La]	0.74	7.6e-05	-0.30	0.26
[Cu/Sr]	0.89	1.7e-09	0.19	0.37	[Ni/Y]	0.72	6.4e-07	0.26	0.13
[Ca/Ba]	0.88	2.3e-12	0.07	0.70	[Ni/Zr]	0.71	6.8e-05	0.26	0.28
[Ni/Sr]	0.87	9.8e-09	-0.36	0.09	[Cu/La]	0.70	3.3e-04	-0.11	0.70
[Na/Y]	0.87	5.4e-12	0.29	0.09	[C/Zr]	0.69	2.2e-04	0.14	0.58
[Co/Ba]	0.87	3.4e-09	0.09	0.68	[Si/La]	0.68	5.4e-04	-0.22	0.41
[Mn/Ba]	0.87	5.1e-12	0.37	0.03	[Mg/La]	0.66	7.8e-04	-0.04	0.90
[Ti/Ba]	0.87	4.1e-12	0.00	0.99	[Mg/Y]	0.64	3.8e-05	0.12	0.49
[C/Ba]	0.86	1.4e-10	0.15	0.42	[Mn/Y]	0.54	7.2e-04	-0.03	0.84
[Si/Ba]	0.86	1.1e-11	0.20	0.25	[C/La]	0.49	2.3e-02	-0.08	0.77
[Mg/Ba]	0.86	2.1e-11	0.14	0.44	[O/Y]	-	-	-	-
[Al/Ba]	0.86	2.0e-08	0.24	0.26	[C/Ce]	-	-	-	-
[Cu/Y]	0.86	1.3e-11	0.30	0.08	[O/Ba]	-	-	-	-
[Na/Ba]	0.85	4.0e-11	0.35	0.04	[Na/Ce]	-	-	-	-
[Mg/Sr]	0.85	8.0e-08	-0.38	0.09	[Ni/Ce]	-	-	-	-
[Cu/Zr]	0.84	2.0e-07	0.35	0.14	[Si/Ce]	-	-	-	-
[Al/Y]	0.82	2.2e-07	-0.10	0.64	[Mg/Ce]	-	-	-	-

Table 5.3: Median and mean absolute deviation (MAD) of the SCC calculated for chemical clocks and [X/Fe], for wide binaries (WBs) and random pairs in Figure 5.2.

		Median	MAD
Chemical clocks	WBs	0.85	0.04
	random pairs	0.15	0.18
[X/Fe]	WBs	0.55	0.13
	random pairs	0.23	0.13

sistent, therefore, they do not only trace chemical homogeneity among wide binaries, they must be carrying age information as well. Moreover, since our sample included some systems whose composition has been subtly affected by different mechanisms (e.g. planet formation, planet engulfment, etc), Figure 5.2 helps us to confirm the idea that chemical clocks are sensitive to the age of the stars regardless of the possible differences in their compositions, and still be consistent between the components of such coeval systems. The reason behind this is that the effect in refractory elements is very small, and affects them almost equally, with a scatter that is generally less than 0.03 dex (e.g. Maia et al., 2019). So, removing this signature from the abundance of the star and deriving the chemical clocks would lead to variations of less than 0.03 dex.

In a different scenario, if we simply consider true that chemical clocks are capable of identifying contemporary systems, our results would confirm that the components of wide binaries are coeval, and it would be one of the first works in the literature to do an analysis with such a large and varied sample.

5.2 The case of HIP 34426/HIP 34407

In previous sections we have checked that stars in wide binaries have homogeneous chemical compositions within the uncertainties. This confirms expectations and previous results (Andrews et al., 2018; Hawkins et al., 2020) since all known plausible formation scenarios indicate that they share common origins, hence they must share their chemical composition, especially if they are on somewhat similar evolutionary states.

All that said, however, the case of HIP 34426/HIP 34407 is puzzling and is worth discussing. From Figure 4.1 we see that abundances are very different (about 0.2 dex), with C and O the only exceptions. These stars were already analyzed by Ramírez et al. (2019), who suggest the differences might be coming from stars not being truly siblings but chance alignments, the birth cloud not being homogeneous, or engulfment of planetary material. After performing an analysis of the astrometry and the radial velocities of the system, they found that HIP 34426 shows a variation in radial velocity of approximately 60 m s^{-1}, something that could indicate the presence of a planet such as a large Jupiter or the existence of a third component of the system. Furthermore, the difference in the total velocity of the system positions it as a physically unbound system, but given its age, Ramírez et al. (2019) propose that it was a binary at formation.

If these stars were not siblings, but instead were (1) formed at separate sites with a difference of about 0.2 dex in metallicity, or (2) sites that suffered the possible effects of chemical evolution (e.g. some considerable time span between the formation of both components) or stellar migration, then, unless a large coincidence, they most likely would have significantly different ages and, therefore, different clocks. However, according to Ramírez et al. (2019) their ages are very consistent, which most likely rules out these possibilities and that of a chance alignment, since the probability for two independent and coeval stars to become a wide binary by dynamical capture in the field is negligible. Furthermore, we see in Figure 5.1 that within the 22 chemical clocks measured in this system, 14 of them show that the system is located almost perfectly on the one-to-one line despite the seemingly remarkable inhomogeneity (for a typical wide binary system) in [X/Fe].

If we take the similarity of the chemical clocks as an indication for the stars in this binary being coeval, then we interpret our results as strong evidence that the cloud material from which they formed was inhomogeneous to these levels, on a scale equivalent to the projected separation of the components of this pair. This may have important implications for the idea of chemical tagging for Galactic archaeology. The case of binary

systems like this stands in stark contrast with the recent detailed study of Kos et al. (2021), who determined chemical abundances of about 300 GALAH stars distributed in the Orion nebula, finding that the nebula is chemically homogeneous (typically within 0.1 dex in each element, except Li), at higher level of precision than the difference observed in the HIP 34426/HIP 34407 system.

Recently, Peñarrubia (2021) proposed that the formation of ultra-wide binaries ($s >$ 0.1 pc) is via chance entrapment of unrelated stars in the tidal streams of disrupting clusters, and found that most pairs formed in tidal streams can easily be disrupted by subtle gravitational interactions with other objects. Here we propose that HIP 34426/HIP 34407 might be part of a tidal stream. This scenario could explain some of the characteristics that we observe in this system, such as its coevality and the astrometric differences that in principle classify it as a non-physically bound system (see Ramírez et al., 2019).

5.3 Systematic uncertainties and applicability of chemical clocks

We are aware that different spectral methodologies can lead to significantly different abundance results (Hinkel et al., 2016; Jofré et al., 2017b, 2019; Jönsson et al., 2018). Our analysis depends on data taken from the literature, and therefore can be affected by systematic uncertainties. One of them is that, in spite of the fact that we used the same linelist for our analysis for the pairs for which we had EWs, H20 derived their chemical abundances using a different selection of lines than ours. Jofré et al. (2019) extensively discuss the effects of line selections in resulting abundances. In particular, while being consistent among all pairs in our full sample, we can see from Figure 5.1 that the ratios [Zn/Ba], [Mg/Ba], [Mn/Ba], and [Cu/Ba] are very different for H20 than the rest of the sample: they show a tendency to negative values, that do not overlap with range of abundances found in Jofré et al. (2020). We note that Jofré et al. (2020) used a sample of stars spanning very young to very old ages, leaving little space for a systematic offset in these abundance ratios due to age.

To investigate this further, in Figure 5.3 we plot the same abundances as in Figure 5.1 but with the pairs colored by the average $T_{\rm eff}$ of the system. It is evident from the plot that the cases of [X/Y] with large range along the 1-1 line, also show a gradient with stellar temperature, i.e. mass. Generally, stars with higher temperatures ($\sim 6000-6200$ K) tend to produce ratios concentrated at lower absolute values than cooler stars. We particularly remark the cases where Ba is involved (e.g. [Ti/Ba], [Si/Ba], [Na/Ba]), showing that there probably is some strong effect depending on the stellar mass for the retrieval of abundances of this element. Moreover hotter stars seem to be more dispersed around the 1-1 line. We recall that the hottest stars are also those analyzed by H20.

It is worth commenting that the stellar temperature has a large impact in the line strength of neutral atomic lines (this is why we adopted the excitation balance method to determine temperature, see Section 3). The line strength can have a particularly large implication in determining abundances which have strong effects due to hyperfine structure splitting (HFS), such as Mn, Co or Ba. The way different methods deal with HFS can indeed be a major source of uncertainty for particular elements like Mn or Co (del Peloso et al., 2005; Jofré et al., 2017b). For stars of different temperatures, abundances of Mn can be very different if different prescriptions for HFS are employed. We also refer to Casamiquela et al. (2020) for the discussions about striking dependencies with $T_{\rm eff}$ (remarkably for Ba, Na, and Mn). The systematic difference in chemical clocks found here is therefore a combination of line selection, HFS treatment and stellar temperature.

There are some discussions in the literature about the metallicity dependency on chemical clocks (e.g. Feltzing et al., 2017; Delgado Mena et al., 2019). Casali et al. (2020) found that the slopes of [Y/Mg] and [Y/Al] versus stellar age change with metallicity (by using steps of ± 0.2 dex in [Fe/H]), and related this to the star formation history of the Milky Way. They concluded that the position of the stars in the Galactic plane is another important parameter to take into account when using chemical clocks to determine ages (e.g. whether it belongs to the thin disk or to the thick disk), because at different locations stars can have different metallicities. Most recently, Casamiquela et al. (2021b)

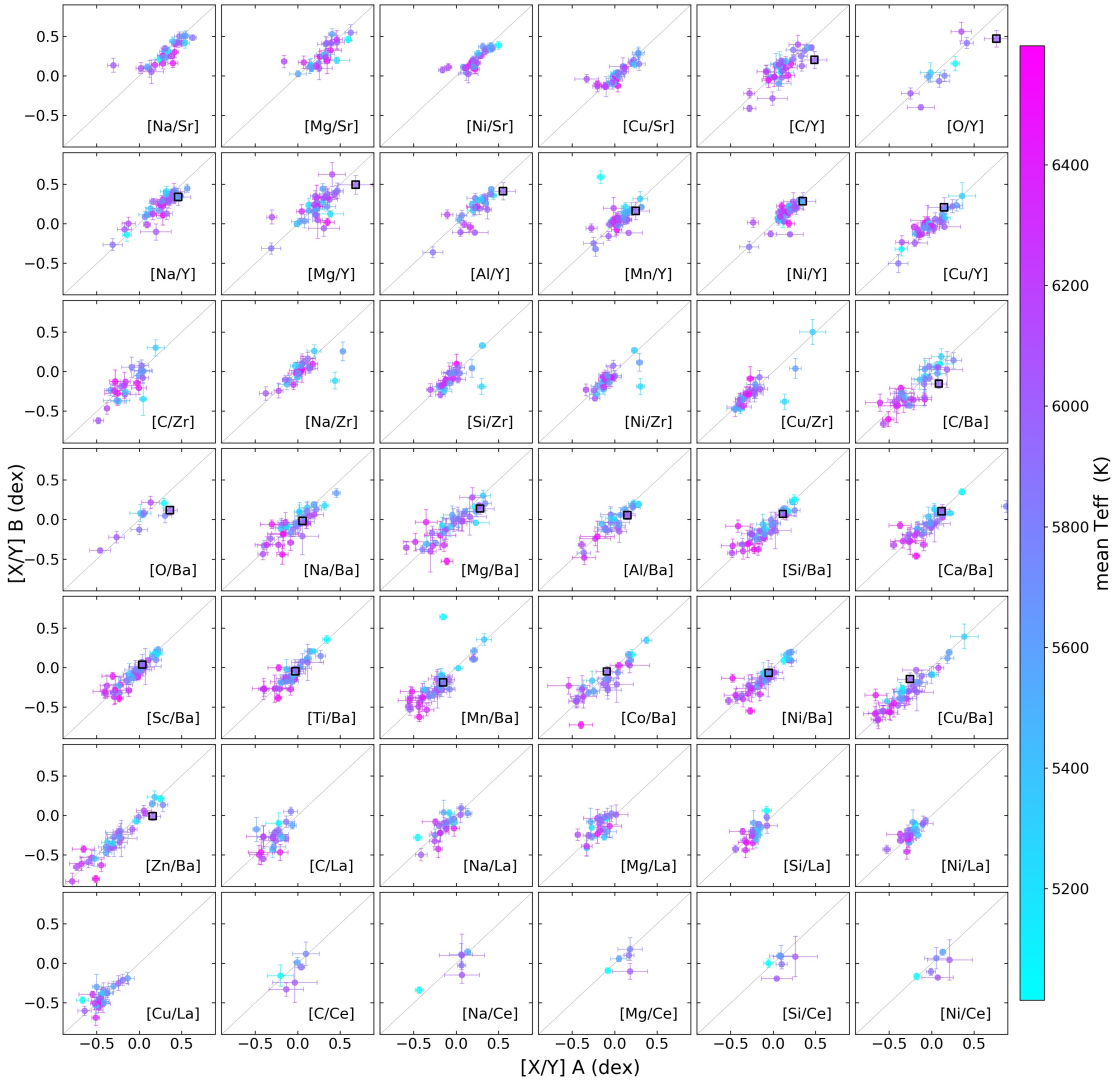

Figure 5.3: Comparison between the components of wide binaries for potential chemical clocks considered in this work. Colors depict the mean temperature of the system. Generally, stars with higher temperatures ($\sim 6000 - 6200$ K) tend to produce ratios concentrated at lower absolute values than cooler stars, and hotter stars seem to be more dispersed around the 1-1 line.

used a sample of red clump stars in 47 open clusters to study the abundance-age relation in a large spatial volume (6 kpc $< R_{\rm CG} <$ 12 kpc), covering regions outside the local bubble, unlike most studies on chemical clocks that use solar twins. By studying [Y/Mg] and [Y/Al] in more detail, they find that the clusters located outside the solar neighborhood appear to have a significantly greater dispersion in abundances compared to the local ones, without finding any dependence on metallicity because of the narrow range in [Fe/H] of their sample. They attribute this finding to galactic dynamics processes, such as radial migration of stars or clusters, which are more likely to be sampled when covering a wider range in distance and can trace different chemical evolutionary histories.

In general, the results of other studies indicate that chemical clocks have several limitations caused by the chemical and dynamic nature of our Milky Way, so one must be very careful when using them to derive ages. Even so, their conclusions do not present problems or restrictions regarding chemical clocks being consistent in coeval star systems. Little however has been discussed in terms of the effects in deriving ages using chemical clocks when such abundances are hampered by systematic uncertainties such as those discussed here. More such analyses are needed in order to fully assess the applicability of chemical clocks for wide Galactic archaeology studies.

5.4 Most consistent clocks in wide binaries

Based on our results we have selected three chemical clocks that have the highest correlation coefficient for wide binaries, low SCC for random pairs (< 0.2), and that also trace the age consistency of HIP 34426/HIP 34407 system despite the chemical differences of its components. Figure 5.4 shows [Sc/Ba], [Ca/Ba] and [Ti/Ba] and the SCC values for wide binaries and random pairs.

We can see that despite coming from independent spectroscopic measurements, the chemical clocks of the wide binaries fit nicely to the 1-1 line, and although we are aware that there are systematic errors in our sample due to the inclusion of systems analyzed

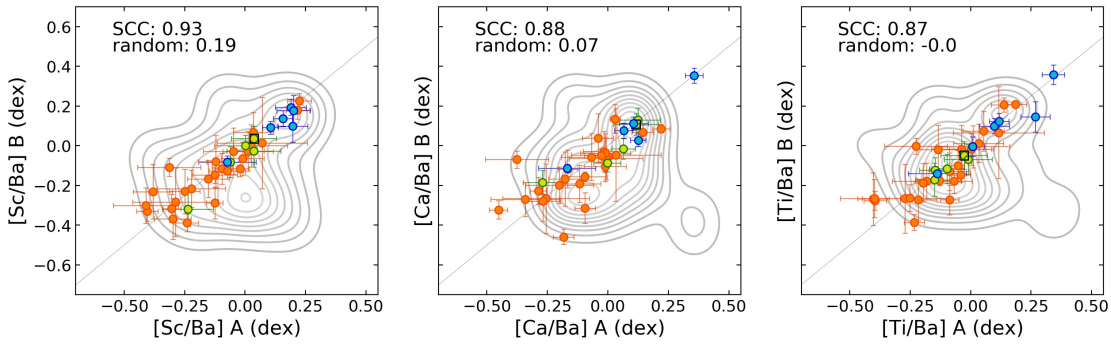

Figure 5.4: Chemical clocks with the higher correlation in our sample of wide binaries: [Sc/Ba], [Ca/Ba] and [Ti, Ba]. The distribution of random pairs is shown in gray curves and HIP 34426/HIP 34407 is marked with a black square, as in Figure 5.1. These abundance ratios can trace the coevality of HIP 34426/HIP 34407, despite its chemical inhomogeneity.

with different methods, these do not affect when plotting the age consistency of these systems. But, if they are to be implemented in chemical tagging studies, it is necessary to follow a spectroscopic analysis as consistent as possible in order to avoid any systematic uncertainty which could make the identification of stellar groups very difficult. It is worth emphasizing that Figure 5.4 shows the potential of these abundance ratios to represent the ages of systems that arise from a common origin, even when certain chemical inhomogeneities are present, but still, it remains to be seen how these clocks relate to the individual ages of the components of wide binaries.

In this chapter we accomplished the main aim of this thesis by finding that chemical clocks are significantly more consistent among wide binaries than random pairs, even when these systems are not perfectly homogeneous in a chemical sense (something that is illustrated in Figure 4.3, and more remarkably by HIP 34426/HIP 34407). Additionally, we find that these abundance ratios are prone to suffer from systematic effects depending on the spectroscopic methodology implemented in the analysis. Despite this, the fact that chemical clocks really trace information about ages and chemical evolution, makes them an interesting ingredient in other applications, for example in the attempts of chemical tagging.

5.5 Testing chemical tagging of Open Clusters with chemical clocks

As extra test, we want to include in this work our first approach to chemical tagging with chemical clocks, for which we decided to use open clusters (OCs), because of their well-known chemical homogeneity and coevality, but also because most of the stars in the disk were born in structures like this and then were released into the field due to Galactic tidal effects that can destroy stellar clusters (Röser et al., 2019; Röser and Schilbach, 2019; Krumholz et al., 2019). The aim of this exercise is to assess whether chemical clocks provide any advantage to this technique. For that we will focus on three main points: (1) can we recover these OCs with chemical tagging only using individual abundances? (2) can chemical clocks improve the performance of chemical tagging in this sample? and finally (3) can we use chemical clocks to decontaminate the recovered groups?

Blanco-Cuaresma et al. (2015) found limitations in recovering OCs with chemical tagging, given some overlapping of these systems in the abundance space, due to, for example, small ranges in metallicity and variations in chemical abundances at different evolutionary stages. There are some other works like the ones of Price-Jones and Bovy (2019) and Price-Jones et al. (2020) (hereafter PJ19 and PJ20) where they performed chemical tagging based on APOGEE data, and found similar overlapping issues when identifying OCs. Yet, as another test that could be done, Ness et al. (2019) proposed using abundances extracted from the cluster's age relations, such as those shown in their work, to reconstruct synthetic clusters and find the implications of the internal dispersion of OCs in chemical tagging.

Recently, Casamiquela et al. (2021a) used a sample of red clump stars with high precision abundances from 31 OCs to again test chemical tagging with HDBSCAN, but they were only able to reconstruct $\sim$29% of the original clusters, with some contamination, even when the internal coherence of the groups was typically 0.03 dex. They found that only those clusters with particular chemical signatures that stand out from the rest of

Table 5.4: Properties of the sample of OCs from Casamiquela et al. (2020).

Cluster	α (deg)	δ (deg)	# members	log age (yr)	D (pc)
Ruprecht 147	289.06	-16.27	24	9.3	284
Hyades	69.66	17.53	62	8.9	48
NGC 2632	143.93	19.24	22	8.85	186

the clusters could be more easily recovered, otherwise, the chemical overlap practically precludes any strong chemical tagging attempt.

All of these studies have in common that they only used individual abundances as input parameters for clustering. This makes the idea of testing the benefits of including chemical clocks in chemical tagging of OCs even more interesting, because despite efforts it is still an open problem.

5.5.1 Methodology

Given that in some of those studies the importance of using a sample of OCs with large number of members and high-precision abundances is highlighted, we decided to use the sample of 3 OCs from Casamiquela et al. (2020) (hereafter C20), composed by Ruprecht 147, the Hyades, and NGC 2632, each of them with more than 20 stars, as shown in Table 5.4. In C20 they derived the radial velocities, stellar atmospheric parameters and chemical abundances of 22 species (Na I, Mg I, Al I, Si I, Ca I, Sc II, Ti, V I, Cr I, Mn I, Fe, Co I, Ni I, Cu I, Y II, Ba II, La II, Ce II, Nd II, and Eu II) for the components of these clusters with high precision (< 0.04 dex on average).

The methodology implemented in this exercise is based on PJ19, where they used DBSCAN (implemented in `scikit-learn`[2]) for clustering in high-dimensional chemical space, because it does not need information about how many groups are expected, instead it only relies on the density of stars in chemical space to find the groups. From now

[2] `https://scikit-learn.org/stable/modules/generated/sklearn.cluster.DBSCAN.html#`

on we set the difference between cluster and group, being clusters those of the original sample and groups those found by DBSCAN.

This clustering algorithm has two important parameters, ϵ and $N_{\rm pts}$. The radius of a star's chemical neighborhood is given by ϵ, which is derived by computing the median of pairwise distances between stars (x_s, x_t) in chemical space, D, multiplied by a normalized ϵ ($\tilde{\epsilon}$) that can go from 0 to 1

$$\epsilon = \tilde{\epsilon} \cdot \text{median}\left(D_{s,t}^{N_{\rm survey}}(x_s, x_t) \right) \tag{5.1}$$

Where $N_{\rm survey}$ is the number of stars in the chemical space. These distances in the chemical space we derived using a Euclidean metric. The number of points, $N_{\rm pts}$ is the minimum number of stars in the ϵ-neighborhood needed to classify certain star as core, boundary or noise. A core star is one that is surrounded by $N_{\rm pts}$ stars within its $\epsilon-$neighborhood, whereas any star that is within this $\epsilon-$neighborhood but is not a core itself is classified as boundary. If the star is not in the $\epsilon-$neighborhood of any core star it is then classified as noise star.

In a simulation aimed to test the performance of the clustering algorithm, there are three quantities useful to assess the model's performance. First the *Homogeneity*, H_i^j, which is 1 if the group g_i only contains members of a specific cluster o_j, meaning there is no contamination from others. Then there is the *Completeness*, C_i^j, that quantifies how many of the stars of a cluster are recovered and how representative of it the group manages to be

$$H_i^j = \frac{\#\text{stars in } g_i \text{ from } o_j}{\#\text{stars in } g_i} \qquad C_i^j = \frac{\#\text{stars in } g_i \text{ from } o_j}{\#\text{stars in } o_i} \tag{5.2}$$

In order to evaluate if a group is recovered we need to set constrains on its values of homogeneity and completeness. In PJ19 they set these thresholds to be 0.7. Then, if the group has homogeneity and completeness larger than 0.7 we claim that it is recovered, and it is included in a subset R. Finally, the recovery fraction (RF) quantifies how many

of the clusters are well reconstructed, and is given by:

$$RF = \frac{\#\text{groups in } R}{\#\text{open clusters}}$$

To create the chemical space we used a data set of abundances based on PJ20, but including some neutron-capture elements, since they are known to be good tracers of chemical evolution. This ended as a 10-dimensional set formed by Mg, Al, Si, Mn, Fe, Ti, Ni, Sc, Y, and Ba. For chemical clocks we constrained the sample to those with SCC larger than 0.8 (see Table 5.2); a total of 14 abundance ratios. Not only that, but also to check the effect of chemical clocks in this process of chemical tagging we implemented 3 different models with different data sets used to create the chemical space:

- Model 1: Only comprised by individual abundances
- Model 2: Only comprised by chemical clocks
- Model 3: Combines individual abundances and chemical clocks

Finally, to find which combination of parameters provides the best performance, we ran DBSCAN with multiple combinations of $\tilde{\epsilon}$ and N_{pts}. For each of them we computed the homogeneity and completeness of each group to then obtain the recovery fraction of that DBSCAN model.

5.5.2 Results

A DBSCAN model is said to perform the best when it has a maximum RF and a number of groups, equal to the number of clusters. In this case, the best performance should be given for $RF = 1$ and a number of groups equal to 3. In Figure 5.5 are shown the RF, number of groups, and the product between these two variables, for each of the DBSCAN models computed with different combinations of $\tilde{\epsilon}$ and N_{pts}. It presents the results for Model 1 (top), Model 2 (center), and Model 3 (bottom). Thanks to the right panels we can identify the combinations for which a DBSCAN model has the best performance as the points with larger values (which in theory should be equal to 3) colored as dark purple dots.

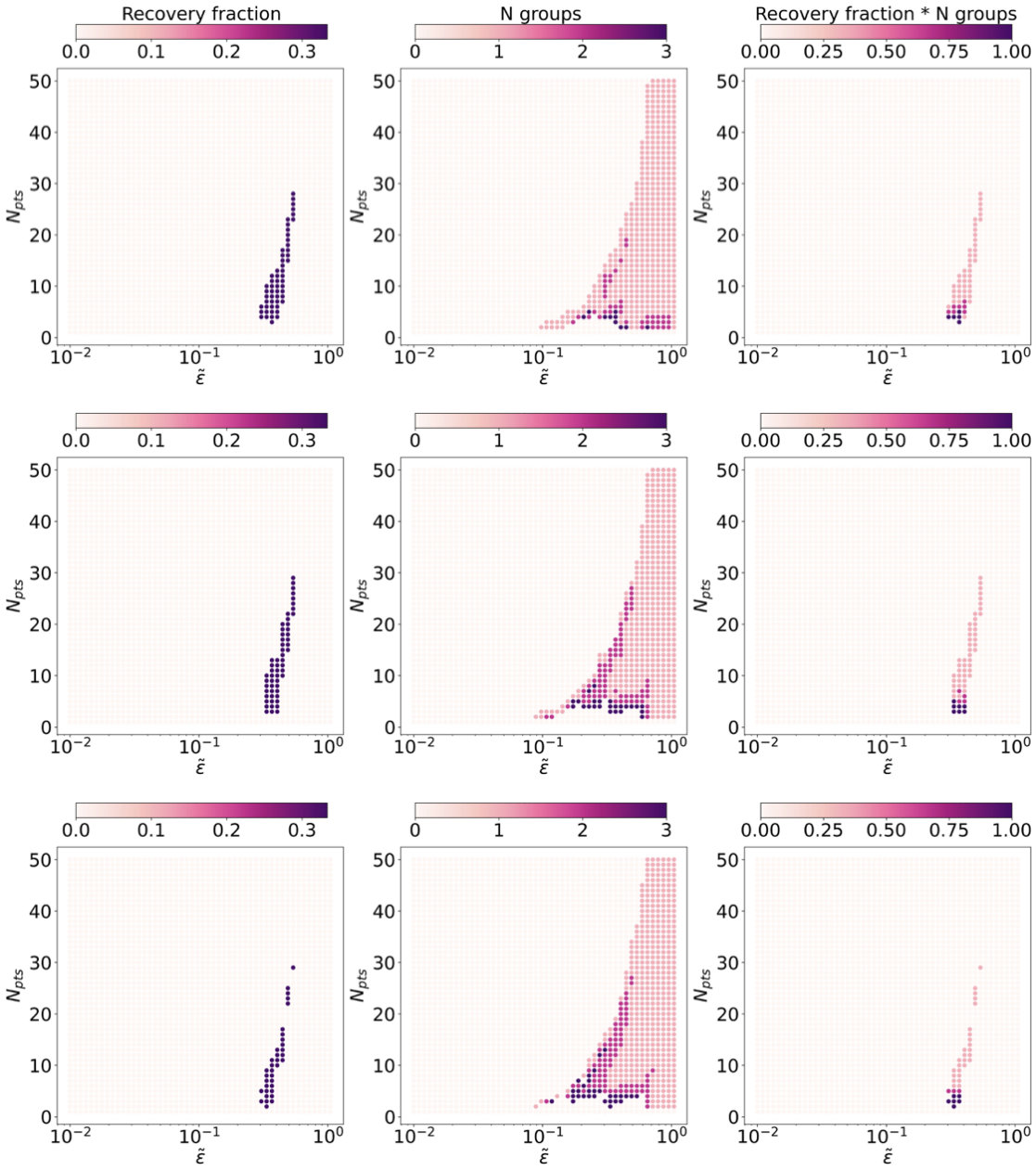

Figure 5.5: Recovery fraction, number of groups, and the product between these two variables, for each of the DBSCAN models computed for different combinations of $\tilde{\epsilon}$ and $N_{\rm pts}$, for the three models: Model 1 (top), Model 2 (center), and Model 3 (bottom). According to the colormap variables with small values are colored as soft pink dots whereas higher values are colored in dark purple.

If we look into the RF values of each DBSCAN model, we can notice that for all three models these do not reach values larger than 0.33, meaning that only one group is recovered in each of them. In all of these models that group had a considerably large fraction of stars from the Hyades (55 of 62 stars, and with 5 stars from NGC 2632 in the best case), thus we can claim that we were able to reconstruct this cluster. The other groups did not meet the homogeneity and completeness conditions to classify them as recovered.

With this information we can answer our first question. We can perform chemical tagging in OCs, but DBCSAN is not able to reconstruct each one of them; only one is well recovered, and happens to be the cluster with the largest number of members of our sample. Furthermore, we find there is no better performance for any combination of data sets since all the models have the practically the same performance. Hence, regarding the second question about whether chemical clocks improve chemical tagging, we must say that it is not the case because for all the models, including those with chemical clocks (Model 2 and 3) the RF is the same, meaning that in this sample clocks did not provide more information that could help to better identify the other two clusters besides the Hyades.

To better understand these results, we must remember that our sample is small and limited in age. There are two clusters, Hyades and NGC 2632, that have similar ages (see Table 5.4), so it could be expected that including chemical clocks in the chemical space would not be useful or sufficient to identify their respective members. Also, since DBSCAN is density sensitive and its threshold is usually given by the densest group in space, it is possible that we could only identify the Hyades and not NGC 2632 because the number of stars in the Hyades is almost three times the number of stars in the sample of NGC 2632. These points illustrate that a better case to study chemical tagging in open clusters could be given by a sample that spans a large range of ages, and (1) has a similar number of members per cluster or (2) the implementation of a clustering algorithm that is not sensitive to cluster density like HDBSCAN.

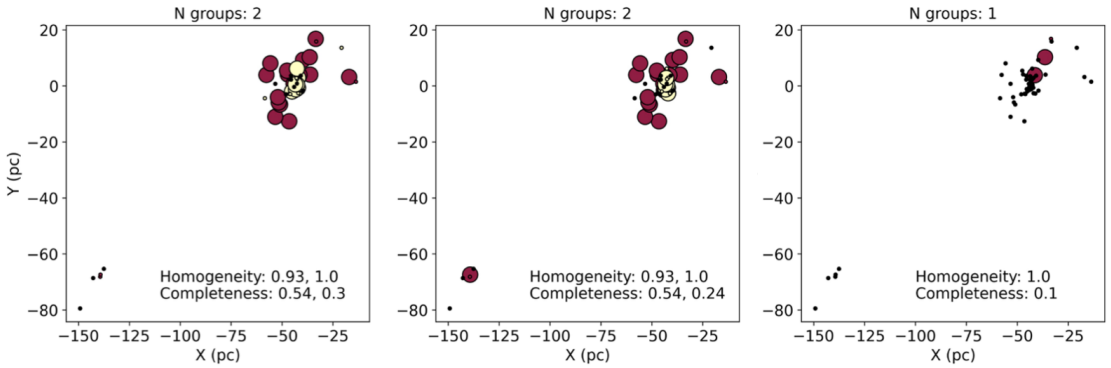

Figure 5.6: Spatial distribution of stars in the groups used for decontamination with chemical clocks. These are examples of the three different results that can be obtained in this exercise: best *(left)*, common *(center)*, and worst *(right)* scenario. Noise stars are depicted as small black circles, while boundary and core stars are small and large yellow or red circles depending on the group they belong to. Each panel shows the homogeneity and completeness of the model. We find that many stars from the cluster are classified as noise, decreasing the completeness in all the cases.

Our final test is to assess if chemical clocks could be used to decontaminate the recovered groups. In order to try this we chose the DBSCAN model with the best performance, which is given with a $N_{\rm pts} = 2$ and $\tilde{\epsilon} = 0.369$ using Model 1. This combination managed to recover a large fraction of the Hyades, a total of 55 members, but with some contamination of 5 stars from NGC 2632, presenting a homogeneity of 0.91 and completeness of 0.81. Since this group presents a new chemical space we had to recompute ϵ, but this time only implementing Model 2. Afterwards, we ran DBSCAN for different combinations of $N_{\rm pts}$ and $\tilde{\epsilon}$ in order to find which provided the best results. Figure 5.6 is a summary of the 3 different cases obtained after trying to decontaminate the group using chemical clocks. It shows each of the stars in the physical space with colors and sizes according to their classification. Stars identified as noise are depicted as small black circles, while boundary stars are shown as small yellow or red circles depending on the group they belong to, and core stars are large circles.

In the left panel is the model obtained with $N_{points} = 6$ and $\tilde{\epsilon} = 0.368$. We see that clocks are able to remove contamination from NGC 2632 (located at the bottom left), but the cluster itself is separated in two different groups. Then, in the middle panel ($N_{points} = 5$ and $\tilde{\epsilon} = 0.335$) we find that the decontamination is not totally efficient

because there still are some stars from NGC 2632 identified as members of the Hyades, and it also separates the group in two. Finally, the worst scenario is shown in the right panel ($N_{points} = 4$ and $\tilde{\epsilon} = 0.19$), and is the one were you get a maximum homogeneity due to the loss of most of the stars that were members of the cluster. We note that in all of these 3 cases the completeness of the group decreases with respect to the value obtained before decontamination, meaning that lots of stars are lost in this process, even stars that are real members of the cluster. Therefore, we can say that decontamination with chemical clocks might work, but it might reduce the number of well-identified stars. Even more, with some combinations of N_{pts} and $\tilde{\epsilon}$ DBSCAN divides the original group in two.

As a summary, after doing this exercise we find that we can use chemical tagging to reconstruct OCs but it has a poor performance. This is expected from the previous results of Blanco-Cuaresma et al. (2015), PJ19, PJ20, and Casamiquela et al. (2021a). Also, we found that chemical clocks do not improve the performance of chemical tagging, but they can be used to decontaminate the recovered groups if we take into account that this will not always provide the cleanest results given the similar ages of OCs. Moreover one has to be aware of the possible loss of real members and possible division inside the cluster itself.

However, there is a lot of room for improvement. One of the keys to have more definitive results would be to have a larger sample of OCs with large number of members, spanning a wider range in age and metallicity, and grouping the stars by their evolutionary stage before trying to chemically tag them, so we can neglect any effects like diffusion which can cause the internal chemical coherence of the cluster to decrease. This is illustrated in C20, where they find abundance amplitudes around 0.15 dex in the Hyades, and 0.2 dex in the other two clusters when using all the stars, independently of their type. Furthermore, in order to make this exercise more realistic, it would be ideal to include field stars, to check to what extent it is possible to differentiate stars that were born together from background stars, similar to the work of Ness et al. (2018), and evaluate if chemical tagging works even when there is some noise in the chemical space.

As mentioned before, implementing clustering algorithms like HDBSCAN would alleviate the need of having a similar number of members for each cluster, and therefore we would not have to worry about the results being biased due to the variety of densities in space. Finally, it would also be interesting to do the same procedure but using different data sets of abundances and chemical clocks, because it is still not clear how the dimensionality of the chemical space can affect the results (see Casamiquela et al., 2021a), and if there is some kind of "recipe" or combination between chemical clocks and abundances that would really allow us to solve the problem of strong chemical tagging in open clusters.

Chapter 6

Summary and future work

In the present work we studied how consistent are abundance ratio groups, collectively known as chemical clocks, among the components of wide binaries. Since the latter are expected to share a common formation site and to be coeval, the comparison of their chemical clocks provides a basic check on the concept itself of a chemical clock and its overall validity. For this, we spectroscopically analyzed a sample of five systems, four of which for the first time, doing a differential analysis with respect to the Sun and using the equivalent widths method. We found that the components of these systems are chemically homogeneous (within 0.1 dex), in good agreement with what has been found in other wide binaries. One remarkable exception is HIP 34426/HIP 34407, which presents differences of ~ 0.2 dex in abundance of most of the elements measured. We found their chemical clocks to be consistent, in agreement with the similarity in their ages that is reported in previous works. With this evidence we discarded some possible formation scenarios which could explain its chemical difference, like stellar migration or a chance alignment.

In order to attempt to test chemical clocks with a bigger and more representative sample of stars, we enlarged our sample by including 31 systems from the literature, finding that the components of these wide binaries follow a 1-1 relation in all the abundance ratios studied, as expected thanks to what we know about the formation scenarios of these systems. Our results indicate that systematic uncertainties from different methodologies

can affect the final abundances, and probably have a significant effect on the different chemical clocks. In order to better assess and quantify this effect, a more careful analysis of common stars but different methods should be performed, as well as having the ages of all these stars.

Also, we compared the degree of correlation of individual abundances and chemical clocks, and found that chemical clocks are more consistent between components of wide binaries than individual abundances, even for stars that might have gone through any process that alter its atmospheric composition. Therefore, we conclude that chemical clocks really carry more information than just the plain run of individual chemical abundances, information probably related to age and a common formation site.

Finally, we propose that including them in the chemical tagging parameter space would be very beneficial and allow better identification of members of disrupted stellar groups. Our first attempt in doing so with a sample of 3 OCs showed us that chemical clocks do not add more information into the chemical space, hence they do not improve the performance of chemical tagging, but they can be used to decontaminate the reconstructed groups carefully, considering possible losses of true members of these clusters. However, testing chemical tagging in OCs has been found to be problematic in other works, so it is important to recall that these are preliminary results and there is a lot of fine-tuning and exercises to do before totally discard any possibility of improvement by using chemical clocks in chemical tagging.

6.1 Future work

As future work we want to study how internal processes in post main sequence (post-MS) stars, such as atomic diffusion (Dotter et al., 2017; Liu et al., 2021), can alter these abundance ratios. For that we can take advantage of the co-natal nature of wide binaries by using systems comprised by a MS and a turn-off (TO) or subgiant (SG) star and compare their chemical clocks.

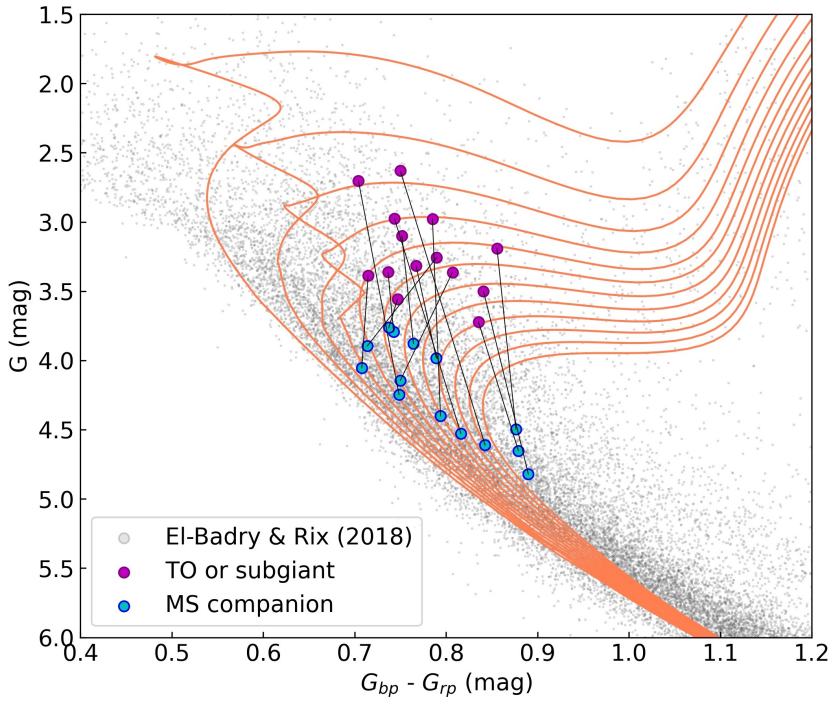

Figure 6.1: Gaia color-magnitude diagram of our sample of wide binaries. The post-MS and MS components are colored purple and cyan, respectively. Also, in order to confirm our evolved components to be so we included isochrones (orange) computed with MIST for solar metallicity ranging from 2 to 13 Gyr with steps of 1 Gyr

Another interesting application of the coeval feature of wide binaries is that we can be able to determine with precision the age of systems in which one of their components is a TO or SG, since at these stages the isochrones are clearly separated from each other and can be easily differentiated. This procedure is able to improve the precision and improve the estimation of the ages of MS stars that are in these types of systems, which we know is highly uncertain via theoretical isochrones, as these barely separate from each other in that stage. Thanks to that we can also use wide binaries formed by a MS and a TO or SG in order to calibrate chemical clocks.

To do so, we already have an accepted proposal to observe 14 of these wide binaries taken from El-Badry and Rix (2018). Our targets and MIST (MESA Isochrones & Stellar Tracks. Paxton et al., 2015; Choi et al., 2016; Dotter, 2016) isochrones from 2 to 13 Gyr are shown in Figure 6.1, where the MS component is colored in blue, the post-MS com-

panion in purple, and the gray background is the full sample of wide binaries of El-Badry and Rix (2018). Due to the pandemic and the consequent closure of some facilities we were not able to observe during the scheduled time. Hopefully we can reschedule these observations to another period, or we can get our proposal accepted again.

Given that wide binaries can span a wide range in metallicity, calibrating chemical clocks with these systems would also allow us to study the metallicity dependence that has been previously found and perhaps contribute to the understanding of how universal these stellar age tracers are.

Appendix A

Additional tables

Table A.1: Astrometry from Gaia EDR3 and stellar parameters of the wide binaries from the literature.

Star	α (deg)	δ (deg)	ϖ (mas)	RV (km s^{-1})	$T_{\rm eff}$ (K)	$\log g$ (dex)	[Fe/H] (dex)	v_{mic} (km s^{-1})
XO-2N	117.03	50.23	6.66	47.68	5307 ± 19	4.30 ± 0.05	0.41 ± 0.02	0.93 ± 0.05
XO-2S	117.03	50.22	6.67	46.85	5374 ± 16	4.33 ± 0.04	0.35 ± 0.02	0.94 ± 0.04
Z2 Ret	49.46	-62.57	83.02	12.21	5854 ± 28	4.54 ± 0.04	-0.22 ± 0.00	0.95 ± 0.09
Z1 Ret	49.57	-62.50	83.06	12.01	5710 ± 22	4.53 ± 0.03	-0.20 ± 0.00	0.80 ± 0.07
HAT-P-4	229.99	36.23	3.11	-1.67	6036 ± 46	4.33 ± 0.13	0.28 ± 0.01	1.29 ± 0.07
TYC 2569	230.00	36.21	3.08	-1.94	6035 ± 36	4.39 ± 0.10	0.18 ± 0.01	1.22 ± 0.06
HD 134439	227.55	-16.40	34.02	310.88	5084 ± 27	4.66 ± 0.06	-1.43 ± 0.02	1.22 ± 0.08
HD 134440	227.55	-16.48	34.03	311.35	4946 ± 26	4.68 ± 0.07	-1.39 ± 0.02	1.17 ± 0.06
HD 20782	50.02	-28.85	27.88	39.89	5789 ± 38	4.41 ± 0.12	-0.02 ± 0.02	1.32 ± 0.10
HD 20781	50.01	-28.78	27.81	40.31	5324 ± 52	4.51 ± 0.10	0.04 ± 0.03	1.02 ± 0.11
WASP-94A	313.78	-34.14	4.75	-8.30	6194 ± 5	4.21 ± 0.01	0.32 ± 0.00	1.43 ± 0.01
WASP-94B	313.79	-34.14	4.72	-8.46	6112 ± 6	4.30 ± 0.02	0.30 ± 0.00	1.32 ± 0.01
WB01A	140.67	50.60	15.15	3.70	5604 ± 24	4.62 ± 0.07	0.36 ± 0.01	0.87 ± 0.05
WB01B	140.66	50.60	15.14	4.16	5663 ± 21	4.67 ± 0.12	0.37 ± 0.01	1.03 ± 0.05
WB02A	203.60	26.28	7.70	-4.76	6460 ± 54	3.96 ± 0.45	-0.11 ± 0.01	1.47 ± 0.08
WB02B	203.60	26.28	7.72	-4.38	6360 ± 95	3.94 ± 0.19	-0.21 ± 0.01	1.62 ± 0.09
WB03A	57.94	34.89	7.33	NaN	6440 ± 38	4.36 ± 0.34	-0.35 ± 0.02	1.09 ± 0.11
WB03B	57.94	34.88	7.33	NaN	6461 ± 64	4.56 ± 0.68	-0.34 ± 0.01	1.47 ± 0.14
WB04A	63.94	45.39	13.03	64.87	5828 ± 31	4.35 ± 0.20	0.00 ± 0.01	1.17 ± 0.05
WB04B	63.94	45.39	13.07	64.73	5886 ± 29	4.44 ± 0.29	0.04 ± 0.01	1.16 ± 0.05
WB05A	53.85	42.31	6.12	16.56	6027 ± 29	4.29 ± 0.31	0.20 ± 0.01	1.25 ± 0.04
WB05B	53.87	42.30	6.08	16.95	5995 ± 68	4.32 ± 0.44	0.09 ± 0.01	1.32 ± 0.05
WB06A	36.23	-2.11	8.27	NaN	6302 ±108	4.22 ± 0.26	-0.20 ± 0.01	1.54 ± 0.07
WB06B	36.22	-2.11	8.27	26.15	6251 ± 52	4.30 ± 0.49	-0.19 ± 0.01	1.36 ± 0.06
WB07A	24.41	7.15	14.62	NaN	5247 ± 22	4.67 ± 0.20	0.14 ± 0.01	0.70 ± 0.04
WB07B	24.42	7.15	14.57	23.81	5250 ± 21	4.56 ± 0.23	0.13 ± 0.01	0.88 ± 0.04
WB08A	26.06	9.49	13.92	6.72	6513 ± 44	4.07 ± 0.85	-0.06 ± 0.01	1.37 ± 0.07
WB08B	26.06	9.48	13.93	6.94	6682 ± 15	4.39 ± 0.49	-0.07 ± 0.02	1.35 ± 0.12
WB09A	25.33	10.11	12.36	17.49	5908 ± 61	4.31 ± 0.28	-0.28 ± 0.01	1.27 ± 0.06
WB09B	25.32	10.11	12.36	18.13	6091 ± 39	4.31 ± 0.39	-0.16 ± 0.01	1.24 ± 0.06
WB10A	65.62	51.81	8.94	NaN	6242 ± 32	4.83 ± 0.28	-0.01 ± 0.01	1.22 ± 0.06
WB10B	65.61	51.81	8.97	NaN	6025 ± 17	4.80 ± 0.28	0.02 ± 0.01	1.02 ± 0.04
WB11A	125.74	7.63	19.66	-15.86	5479 ± 65	4.78 ± 0.33	-0.01 ± 0.01	1.52 ± 0.05
WB11B	125.75	7.63	19.67	-15.56	5355 ± 57	4.75 ± 0.01	-0.06 ± 0.01	1.20 ± 0.05
WB12A	112.43	18.28	8.21	-26.25	5913 ± 24	4.21 ± 0.17	-0.20 ± 0.01	1.13 ± 0.05
WB12B	112.45	18.28	8.22	-26.79	5916 ± 14	4.27 ± 0.25	-0.16 ± 0.01	1.04 ± 0.04
WB13A	69.36	0.58	15.67	38.97	5864 ± 69	3.92 ± 0.10	-0.30 ± 0.01	1.37 ± 0.06
WB13B	69.36	0.55	15.70	38.61	5865 ± 24	3.79 ± 0.21	-0.33 ± 0.01	1.31 ± 0.08
WB14A	73.57	7.37	33.78	46.67	5193 ± 68	4.50 ± 0.44	0.07 ± 0.01	1.22 ± 0.04
WB14B	73.57	7.37	33.76	46.54	5226 ± 38	4.65 ± 0.07	0.06 ± 0.01	1.13 ± 0.04
WB15A	77.56	14.00	9.70	36.86	6519 ± 65	4.38 ± 0.26	0.13 ± 0.01	1.57 ± 0.09
WB15B	77.56	14.00	9.70	NaN	6493 ± 69	4.34 ± 0.31	0.12 ± 0.01	1.55 ± 0.08

Table A.2: *Continuation of Table A.1*

Star	α (deg)	δ (deg)	ϖ (mas)	RV (km s^{-1})	$T_{\rm eff}$ (K)	$\log g$ (dex)	[Fe/H] (dex)	v_{mic} (km s^{-1})
WB16A	177.00	-8.63	7.34	-16.74	6258 ± 47	4.13 ± 0.26	-0.30 ± 0.01	1.39 ± 0.09
WB16B	177.00	-8.63	7.33	-17.04	6354 ± 51	4.44 ± 0.49	-0.17 ± 0.01	1.31 ± 0.10
WB17A	209.03	-4.62	8.95	NaN	6095 ±106	4.06 ± 0.34	0.00 ± 0.02	1.55 ± 0.09
WB17B	209.03	-4.62	8.94	8.66	6265 ± 83	4.15 ± 0.34	0.01 ± 0.01	1.71 ± 0.07
WB18A	156.78	18.06	17.49	11.04	5347 ± 64	4.60 ± 0.32	0.07 ± 0.01	1.10 ± 0.04
WB18B	156.78	18.06	17.50	NaN	5404 ± 17	4.64 ± 0.32	0.05 ± 0.01	1.05 ± 0.03
WB19A	178.63	19.41	25.38	5.94	5739 ± 25	4.69 ± 0.23	-0.07 ± 0.01	1.00 ± 0.05
WB19B	178.64	19.43	25.38	5.76	5607 ± 14	4.75 ± 0.12	-0.04 ± 0.01	0.76 ± 0.05
WB20A	174.71	32.64	7.52	21.61	6195 ± 25	4.47 ± 0.30	-0.16 ± 0.01	1.10 ± 0.06
WB20B	174.68	32.63	7.57	22.07	6283 ± 26	4.55 ± 0.30	-0.14 ± 0.01	1.19 ± 0.06
WB21A	46.01	52.52	7.22	-40.73	5947 ±129	4.16 ± 0.23	-0.66 ± 0.01	1.59 ± 0.15
WB21B	46.01	52.52	7.22	NaN	6040 ± 45	4.21 ± 0.31	-0.58 ± 0.01	1.20 ± 0.13
WB22A	75.89	63.09	31.11	-26.02	5514 ± 26	4.64 ± 0.21	-0.22 ± 0.01	1.01 ± 0.05
WB22B	75.88	63.08	31.16	-26.50	5687 ± 25	4.57 ± 0.38	-0.21 ± 0.01	1.06 ± 0.04
WB23A	137.10	27.54	20.58	30.02	5996 ± 30	4.62 ± 0.22	-0.26 ± 0.01	1.07 ± 0.06
WB23B	137.11	27.54	20.45	30.31	5974 ± 68	4.51 ± 0.33	-0.28 ± 0.01	1.30 ± 0.05
WB24A	159.87	31.71	14.43	8.66	5632 ± 45	4.63 ± 0.35	0.17 ± 0.01	1.13 ± 0.04
WB24B	159.86	31.70	14.45	7.64	5605 ± 50	4.63 ± 0.38	0.19 ± 0.01	1.17 ± 0.04
WB25A	126.71	39.01	11.79	-4.39	6430 ± 37	4.59 ± 0.23	-0.04 ± 0.01	1.28 ± 0.07
WB25B	126.64	39.05	11.83	-3.31	6232 ± 34	4.64 ± 0.20	-0.10 ± 0.01	1.29 ± 0.09

Table A.3: NLTE corrections of each line of the oxygen triplet, extracted from MPIA.

Star	7771.959 (Å)	7774.177 (Å)	7775.398 (Å)
HIP 32865	-0.740	-0.698	-0.643
HIP 32871	-0.831	-0.783	-0.717
HIP 34407	-0.841	-0.785	-0.709
HIP 34426	-0.792	-0.724	-0.641
HIP 52792	-0.981	-0.921	-0.825
HIP 52793	-0.827	-0.765	-0.682
HIP 58240	-0.684	-0.645	-0.600
HIP 58241	-0.689	-0.650	-0.603
HIP 15310	-0.797	-0.788	-0.772
HIP 15304	-0.893	-0.891	-0.890
VESTA	-0.743	-0.710	-0.668

Bibliography

Adibekyan, V., Delgado-Mena, E., Figueira, P., Sousa, S. G., Santos, N. C., Faria, J. P., González Hernández, J. I., Israelian, G., Harutyunyan, G., Suárez-Andrés, L., and Hakobyan, A. A. (2016). ζ^2 Reticuli, its debris disk, and its lonely stellar companion ζ^1 Ret. Different T_c trends for different spectra. A&A, 591:A34.

Andrews, J. J., Anguiano, B., Chanamé, J., Agüeros, M. A., Lewis, H. M., Hayes, C. R., and Majewski, S. R. (2019). Using APOGEE Wide Binaries to Test Chemical Tagging with Dwarf Stars. ApJ, 871(1):42.

Andrews, J. J., Chanamé, J., and Agüeros, M. A. (2018). Wide binaries in Tycho-Gaia II: metallicities, abundances and prospects for chemical tagging. MNRAS, 473(4):5393–5406.

Asplund, M., Grevesse, N., and Sauval, A. J. (2005). The Solar Chemical Composition. In Barnes, Thomas G., I. and Bash, F. N., editors, *Cosmic Abundances as Records of Stellar Evolution and Nucleosynthesis*, volume 336 of *Astronomical Society of the Pacific Conference Series*, page 25.

Barnes, S. A. (2003). On the Rotational Evolution of Solar- and Late-Type Stars, Its Magnetic Origins, and the Possibility of Stellar Gyrochronology. ApJ, 586(1):464–479.

Barnes, S. A. (2007). Ages for Illustrative Field Stars Using Gyrochronology: Viability, Limitations, and Errors. ApJ, 669(2):1167–1189.

Battistini, C. and Bensby, T. (2015). The origin and evolution of the odd-Z iron-peak elements Sc, V, Mn, and Co in the Milky Way stellar disk. A&A, 577:A9.

Bedell, M., Bean, J. L., Meléndez, J., Spina, L., Ramírez, I., Asplund, M., Alves-Brito, A., dos Santos, L., Dreizler, S., Yong, D., Monroe, T., and Casagrande, L. (2018). The Chemical Homogeneity of Sun-like Stars in the Solar Neighborhood. ApJ, 865(1):68.

Bergemann, M. and Cescutti, G. (2010). Chromium: NLTE abundances in metal-poor stars and nucleosynthesis in the Galaxy. A&A, 522:A9.

Bernstein, R., Shectman, S. A., Gunnels, S. M., Mochnacki, S., and Athey, A. E. (2003). MIKE: A Double Echelle Spectrograph for the Magellan Telescopes at Las Campanas Observatory. In Iye, M. and Moorwood, A. F. M., editors, *Instrument Design and Performance for Optical/Infrared Ground-based Telescopes*, volume 4841 of *Society of Photo-Optical Instrumentation Engineers (SPIE) Conference Series*, pages 1694–1704.

Blanco-Cuaresma, S. (2019). Modern stellar spectroscopy caveats. MNRAS, 486(2):2075–2101.

Blanco-Cuaresma, S., Soubiran, C., Heiter, U., Asplund, M., Carraro, G., Costado, M. T., Feltzing, S., González-Hernández, J. I., Jiménez-Esteban, F., Korn, A. J., Marino, A. F., Montes, D., San Roman, I., Tabernero, H. M., and Tautvaišienė, G. (2015). Testing the chemical tagging technique with open clusters. A&A, 577:A47.

Blanco-Cuaresma, S., Soubiran, C., Heiter, U., and Jofré, P. (2014). Determining stellar atmospheric parameters and chemical abundances of FGK stars with iSpec. A&A, 569:A111.

Bodaghee, A., Santos, N. C., Israelian, G., and Mayor, M. (2003). Chemical abundances of planet-host stars. Results for alpha and Fe-group elements. A&A, 404:715–727.

Caffau, E., Ludwig, H. G., Bonifacio, P., Faraggiana, R., Steffen, M., Freytag, B., Kamp, I., and Ayres, T. R. (2010). The solar photospheric abundance of carbon. Analysis of atomic carbon lines with the CO5BOLD solar model. A&A, 514:A92.

Casali, G., Spina, L., Magrini, L., Karakas, A. I., Kobayashi, C., Casey, A. R., Feltzing, S., Van der Swaelmen, M., Tsantaki, M., Jofré, P., Bragaglia, A., Feuillet, D., Bensby, T., Biazzo, K., Gonneau, A., Tautvaišienė, G., Baratella, M., Roccatagliata, V., Pancino, E., Sousa, S., Adibekyan, V., Martell, S., Bayo, A., Jackson, R. J., Jeffries, R. D.,

Gilmore, G., Randich, S., Alfaro, E., Koposov, S. E., Korn, A. J., Recio-Blanco, A., Smiljanic, R., Franciosini, E., Hourihane, A., Monaco, L., Morbidelli, L., Sacco, G., Worley, C., and Zaggia, S. (2020). The Gaia-ESO survey: the non-universality of the age-chemical-clocks-metallicity relations in the Galactic disc. A&A, 639:A127.

Casamiquela, L., Castro-Ginard, A., Anders, F., and Soubiran, C. (2021a). The (im)possibility of strong chemical tagging. *arXiv e-prints*, page arXiv:2108.13431.

Casamiquela, L., Soubiran, C., Jofré, P., Chiappini, C., Lagarde, N., Tarricq, Y., Carrera, R., Jordi, C., Balaguer-Núñez, L., Carbajo-Hijarrubia, J., and Blanco-Cuaresma, S. (2021b). Abundance-age relations with red clump stars in open clusters. A&A, 652:A25.

Casamiquela, L., Tarricq, Y., Soubiran, C., Blanco-Cuaresma, S., Jofré, P., Heiter, U., and Tucci Maia, M. (2020). Differential abundances of open clusters and their tidal tails: Chemical tagging and chemical homogeneity. A&A, 635:A8.

Chambers, J. (2010). *in Exoplanets*, pages 297–317. Tucson, AZ: University of Arizona Press.

Chanamé, J. and Gould, A. (2004). Disk and Halo Wide Binaries from the Revised Luyten Catalog: Probes of Star Formation and MACHO Dark Matter. ApJ, 601(1):289–310.

Chanamé, J. and Ramírez, I. (2012). Toward Precise Ages for Single Stars in the Field. Gyrochronology Constraints at Several Gyr Using Wide Binaries. I. Ages for Initial Sample. ApJ, 746(1):102.

Chaplin, W. J. and Miglio, A. (2013). Asteroseismology of Solar-Type and Red-Giant Stars. ARA&A, 51(1):353–392.

Choi, J., Dotter, A., Conroy, C., Cantiello, M., Paxton, B., and Johnson, B. D. (2016). Mesa Isochrones and Stellar Tracks (MIST). I. Solar-scaled Models. ApJ, 823(2):102.

da Silva, R., Porto de Mello, G. F., Milone, A. C., da Silva, L., Ribeiro, L. S., and Rocha-Pinto, H. J. (2012). Accurate and homogeneous abundance patterns in solar-type stars of the solar neighbourhood: a chemo-chronological analysis. A&A, 542:A84.

del Peloso, E. F., Cunha, K., da Silva, L., and Porto de Mello, G. F. (2005). Abundances of Mn, Co and Eu in a sample of 20 F-G disk stars: the influence of hyperfine structure splitting. A&A, 441(3):1149–1156.

Delgado Mena, E., Moya, A., Adibekyan, V., Tsantaki, M., González Hernández, J. I., Israelian, G., Davies, G. R., Chaplin, W. J., Sousa, S. G., Ferreira, A. C. S., and Santos, N. C. (2019). Abundance to age ratios in the HARPS-GTO sample with Gaia DR2. Chemical clocks for a range of [Fe/H]. A&A, 624:A78.

Desidera, S., Gratton, R. G., Lucatello, S., and Claudi, R. U. (2006). Abundance difference between components of wide binaries. II. The southern sample. A&A, 454(2):581–593.

Dotter, A. (2016). MESA Isochrones and Stellar Tracks (MIST) 0: Methods for the Construction of Stellar Isochrones. ApJS, 222(1):8.

Dotter, A., Conroy, C., Cargile, P., and Asplund, M. (2017). The Influence of Atomic Diffusion on Stellar Ages and Chemical Tagging. ApJ, 840(2):99.

Eiroa, C., Fedele, D., Maldonado, J., González-García, B. M., Rodmann, J., Heras, A. M., Pilbratt, G. L., Augereau, J. C., Mora, A., Montesinos, B., Ardila, D., Bryden, G., Liseau, R., Stapelfeldt, K., Launhardt, R., Solano, E., Bayo, A., Absil, O., Arévalo, M., Barrado, D., Beichmann, C., Danchi, W., Del Burgo, C., Ertel, S., Fridlund, M., Fukagawa, M., Gutiérrez, R., Grün, E., Kamp, I., Krivov, A., Lebreton, J., Löhne, T., Lorente, R., Marshall, J., Martínez-Arnáiz, R., Meeus, G., Montes, D., Morbidelli, A., Müller, S., Mutschke, H., Nakagawa, T., Olofsson, G., Ribas, I., Roberge, A., Sanz-Forcada, J., Thébault, P., Walker, H., White, G. J., and Wolf, S. (2010). Cold DUst around NEarby Stars (DUNES). First results. A resolved exo-Kuiper belt around the solar-like star ζ^2 Ret. A&A, 518:L131.

El-Badry, K. and Rix, H.-W. (2018). Imprints of white dwarf recoil in the separation distribution of Gaia wide binaries. MNRAS, 480(4):4884–4902.

Elliott, P. and Bayo, A. (2016). The crucial role of higher order multiplicity in wide binary formation: a case study using the β-Pictoris moving group. MNRAS, 459(4):4499–4507.

Feltzing, S., Howes, L. M., McMillan, P. J., and Stonkutė, E. (2017). On the metallicity dependence of the [Y/Mg]-age relation for solar-type stars. MNRAS, 465(1):L109–L113.

Fishlock, C. K., Karakas, A. I., Lugaro, M., and Yong, D. (2014). Evolution and Nucleosynthesis of Asymptotic Giant Branch Stellar Models of Low Metallicity. ApJ, 797(1):44.

Freeman, K. and Bland-Hawthorn, J. (2002). The New Galaxy: Signatures of Its Formation. ARA&A, 40:487–537.

Gaia Collaboration, Brown, A. G. A., Vallenari, A., Prusti, T., de Bruijne, J. H. J., Babusiaux, C., Biermann, M., Creevey, O. L., Evans, D. W., Eyer, L., Hutton, A., Jansen, F., Jordi, C., Klioner, S. A., Lammers, U., Lindegren, L., Luri, X., Mignard, F., Panem, C., Pourbaix, D., Randich, S., Sartoretti, P., Soubiran, C., Walton, N. A., Arenou, F., Bailer-Jones, C. A. L., Bastian, U., Cropper, M., Drimmel, R., Katz, D., Lattanzi, M. G., van Leeuwen, F., Bakker, J., Cacciari, C., Castañeda, J., De Angeli, F., Ducourant, C., Fabricius, C., Fouesneau, M., Frémat, Y., Guerra, R., Guerrier, A., Guiraud, J., Jean-Antoine Piccolo, A., Masana, E., Messineo, R., Mowlavi, N., Nicolas, C., Nienartowicz, K., Pailler, F., Panuzzo, P., Riclet, F., Roux, W., Seabroke, G. M., Sordo, R., Tanga, P., Thévenin, F., Gracia-Abril, G., Portell, J., Teyssier, D., Altmann, M., Andrae, R., Bellas-Velidis, I., Benson, K., Berthier, J., Blomme, R., Brugaletta, E., Burgess, P. W., Busso, G., Carry, B., Cellino, A., Cheek, N., Clementini, G., Damerdji, Y., Davidson, M., Delchambre, L., Dell'Oro, A., Fernández-Hernández, J., Galluccio, L., García-Lario, P., Garcia-Reinaldos, M., González-Núñez, J., Gosset, E., Haigron, R., Halbwachs, J. L., Hambly, N. C., Harrison, D. L., Hatzidimitriou, D., Heiter, U., Hernández, J., Hestroffer, D., Hodgkin, S. T., Holl, B., Janßen, K., Jevardat de Fombelle, G., Jordan, S., Krone-Martins, A., Lanzafame, A. C., Löffler, W., Lorca, A., Manteiga, M., Marchal, O., Marrese, P. M., Moitinho, A., Mora, A., Muinonen, K., Osborne, P., Pancino, E., Pauwels, T., Petit, J. M., Recio-Blanco,

A., Richards, P. J., Riello, M., Rimoldini, L., Robin, A. C., Roegiers, T., Rybizki, J., Sarro, L. M., Siopis, C., Smith, M., Sozzetti, A., Ulla, A., Utrilla, E., van Leeuwen, M., van Reeven, W., Abbas, U., Abreu Aramburu, A., Accart, S., Aerts, C., Aguado, J. J., Ajaj, M., Altavilla, G., Álvarez, M. A., Álvarez Cid-Fuentes, J., Alves, J., Anderson, R. I., Anglada Varela, E., Antoja, T., Audard, M., Baines, D., Baker, S. G., Balaguer-Núñez, L., Balbinot, E., Balog, Z., Barache, C., Barbato, D., Barros, M., Barstow, M. A., Bartolomé, S., Bassilana, J. L., Bauchet, N., Baudesson-Stella, A., Becciani, U., Bellazzini, M., Bernet, M., Bertone, S., Bianchi, L., Blanco-Cuaresma, S., Boch, T., Bombrun, A., Bossini, D., Bouquillon, S., Bragaglia, A., Bramante, L., Breedt, E., Bressan, A., Brouillet, N., Bucciarelli, B., Burlacu, A., Busonero, D., Butkevich, A. G., Buzzi, R., Caffau, E., Cancelliere, R., Cánovas, H., Cantat-Gaudin, T., Carballo, R., Carlucci, T., Carnerero, M. I., Carrasco, J. M., Casamiquela, L., Castellani, M., Castro-Ginard, A., Castro Sampol, P., Chaoul, L., Charlot, P., Chemin, L., Chiavassa, A., Cioni, M. R. L., Comoretto, G., Cooper, W. J., Cornez, T., Cowell, S., Crifo, F., Crosta, M., Crowley, C., Dafonte, C., Dapergolas, A., David, M., David, P., de Laverny, P., De Luise, F., De March, R., De Ridder, J., de Souza, R., de Teodoro, P., de Torres, A., del Peloso, E. F., del Pozo, E., Delbo, M., Delgado, A., Delgado, H. E., Delisle, J. B., Di Matteo, P., Diakite, S., Diener, C., Distefano, E., Dolding, C., Eappachen, D., Edvardsson, B., Enke, H., Esquej, P., Fabre, C., Fabrizio, M., Faigler, S., Fedorets, G., Fernique, P., Fienga, A., Figueras, F., Fouron, C., Fragkoudi, F., Fraile, E., Franke, F., Gai, M., Garabato, D., Garcia-Gutierrez, A., García-Torres, M., Garofalo, A., Gavras, P., Gerlach, E., Geyer, R., Giacobbe, P., Gilmore, G., Girona, S., Giuffrida, G., Gomel, R., Gomez, A., Gonzalez-Santamaria, I., González-Vidal, J. J., Granvik, M., Gutiérrez-Sánchez, R., Guy, L. P., Hauser, M., Haywood, M., Helmi, A., Hidalgo, S. L., Hilger, T., Hładczuk, N., Hobbs, D., Holland, G., Huckle, H. E., Jasniewicz, G., Jonker, P. G., Juaristi Campillo, J., Julbe, F., Karbevska, L., Kervella, P., Khanna, S., Kochoska, A., Kontizas, M., Kordopatis, G., Korn, A. J., Kostrzewa-Rutkowska, Z., Kruszyńska, K., Lambert, S., Lanza, A. F., Lasne, Y., Le Campion, J. F., Le Fustec, Y., Lebreton, Y., Lebzelter, T., Leccia, S., Leclerc, N., Lecoeur-Taibi, I., Liao, S., Licata, E., Lindstrøm, E. P., Lister, T. A., Livanou, E., Lobel, A., Madrero Pardo, P., Managau, S., Mann, R. G., Marchant, J. M., Marconi,

M., Marcos Santos, M. M. S., Marinoni, S., Marocco, F., Marshall, D. J., Martin Polo, L., Martín-Fleitas, J. M., Masip, A., Massari, D., Mastrobuono-Battisti, A., Mazeh, T., McMillan, P. J., Messina, S., Michalik, D., Millar, N. R., Mints, A., Molina, D., Molinaro, R., Molnár, L., Montegriffo, P., Mor, R., Morbidelli, R., Morel, T., Morris, D., Mulone, A. F., Munoz, D., Muraveva, T., Murphy, C. P., Musella, I., Noval, L., Ordénovic, C., Orrù, G., Osinde, J., Pagani, C., Pagano, I., Palaversa, L., Palicio, P. A., Panahi, A., Pawlak, M., Peñalosa Esteller, X., Penttilä, A., Piersimoni, A. M., Pineau, F. X., Plachy, E., Plum, G., Poggio, E., Poretti, E., Poujoulet, E., Prša, A., Pulone, L., Racero, E., Ragaini, S., Rainer, M., Raiteri, C. M., Rambaux, N., Ramos, P., Ramos-Lerate, M., Re Fiorentin, P., Regibo, S., Reylé, C., Ripepi, V., Riva, A., Rixon, G., Robichon, N., Robin, C., Roelens, M., Rohrbasser, L., Romero-Gómez, M., Rowell, N., Royer, F., Rybicki, K. A., Sadowski, G., Sagristà Sellés, A., Sahlmann, J., Salgado, J., Salguero, E., Samaras, N., Sanchez Gimenez, V., Sanna, N., Santoveña, R., Sarasso, M., Schultheis, M., Sciacca, E., Segol, M., Segovia, J. C., Ségransan, D., Semeux, D., Shahaf, S., Siddiqui, H. I., Siebert, A., Siltala, L., Slezak, E., Smart, R. L., Solano, E., Solitro, F., Souami, D., Souchay, J., Spagna, A., Spoto, F., Steele, I. A., Steidelmüller, H., Stephenson, C. A., Süveges, M., Szabados, L., Szegedi-Elek, E., Taris, F., Tauran, G., Taylor, M. B., Teixeira, R., Thuillot, W., Tonello, N., Torra, F., Torra, J., Turon, C., Unger, N., Vaillant, M., van Dillen, E., Vanel, O., Vecchiato, A., Viala, Y., Vicente, D., Voutsinas, S., Weiler, M., Wevers, T., Wyrzykowski, Ł., Yoldas, A., Yvard, P., Zhao, H., Zorec, J., Zucker, S., Zurbach, C., and Zwitter, T. (2021). Gaia Early Data Release 3. Summary of the contents and survey properties. A&A, 649:A1.

Godoy Rivera, D. (2021). Exploring Gyrochronology with Young Clusters, Field Binaries, and Post-MS Stars in the Gaia Era. In *American Astronomical Society Meeting Abstracts*, volume 53 of *American Astronomical Society Meeting Abstracts*, page 415.06D.

Gould, A. and Chanamé, J. (2004). New Hipparcos-based Parallaxes for 424 Faint Stars. ApJS, 150(2):455–464.

Gray, D. F. (2008). *The Observation and Analysis of Stellar Photospheres*. Cambridge: Cambridge Univ. Press.

Grevesse, N., Asplund, M., and Sauval, A. J. (2007). The Solar Chemical Composition. Space Sci. Rev., 130(1-4):105–114.

Gustafsson, B., Edvardsson, B., Eriksson, K., Jørgensen, U. G., Nordlund, Å., and Plez, B. (2008). A grid of MARCS model atmospheres for late-type stars. I. Methods and general properties. A&A, 486(3):951–970.

Hawkins, K., Lucey, M., Ting, Y.-S., Ji, A., Katzberg, D., Thompson, M., El-Badry, K., Teske, J., Nelson, T., and Carrillo, A. (2020). Identical or fraternal twins? The chemical homogeneity of wide binaries from Gaia DR2. MNRAS, 492(1):1164–1179.

Haynes, C. J. and Kobayashi, C. (2019). Galactic simulations of r-process elemental abundances. MNRAS, 483(4):5123–5134.

Heiter, U., Lind, K., Bergemann, M., Asplund, M., Mikolaitis, Š., Barklem, P. S., Masseron, T., de Laverny, P., Magrini, L., Edvardsson, B., Jönsson, H., Pickering, J. C., Ryde, N., Bayo Arán, A., Bensby, T., Casey, A. R., Feltzing, S., Jofré, P., Korn, A. J., Pancino, E., Damiani, F., Lanzafame, A., Lardo, C., Monaco, L., Morbidelli, L., Smiljanic, R., Worley, C., Zaggia, S., Randich, S., and Gilmore, G. F. (2021). Atomic data for the Gaia-ESO Survey. A&A, 645:A106.

Hinkel, N. R., Young, P. A., Pagano, M. D., Desch, S. J., Anbar, A. D., Adibekyan, V., Blanco-Cuaresma, S., Carlberg, J. K., Delgado Mena, E., Liu, F., Nordlander, T., Sousa, S. G., Korn, A., Gruyters, P., Heiter, U., Jofré, P., Santos, N. C., and Soubiran, C. (2016). A Comparison of Stellar Elemental Abundance Techniques and Measurements. ApJS, 226(1):4.

Jackson, H., Jofré, P., Yaxley, K., Das, P., de Brito Silva, D., and Foley, R. (2021). Using heritability of stellar chemistry to reveal the history of the Milky Way. MNRAS, 502(1):32–47.

Jofré, P., Das, P., Bertranpetit, J., and Foley, R. (2017a). Cosmic phylogeny: reconstructing the chemical history of the solar neighbourhood with an evolutionary tree. MNRAS, 467(1):1140–1153.

Jofré, P., Heiter, U., and Soubiran, C. (2019). Accuracy and Precision of Industrial Stellar Abundances. ARA&A, 57:571–616.

Jofré, P., Heiter, U., Soubiran, C., Blanco-Cuaresma, S., Masseron, T., Nordlander, T., Chemin, L., Worley, C. C., Van Eck, S., Hourihane, A., Gilmore, G., Adibekyan, V., Bergemann, M., Cantat-Gaudin, T., Delgado-Mena, E., González Hernández, J. I., Guiglion, G., Lardo, C., de Laverny, P., Lind, K., Magrini, L., Mikolaitis, S., Montes, D., Pancino, E., Recio-Blanco, A., Sordo, R., Sousa, S., Tabernero, H. M., and Vallenari, A. (2015). Gaia FGK benchmark stars: abundances of α and iron-peak elements. A&A, 582:A81.

Jofré, P., Heiter, U., Tucci Maia, M., Soubiran, C., Worley, C. C., Hawkins, K., Blanco-Cuaresma, S., and Rodrigo, C. (2018). The Gaia FGK Benchmark Stars Version 2.1. *Research Notes of the American Astronomical Society*, 2(3):152.

Jofré, P., Heiter, U., Worley, C. C., Blanco-Cuaresma, S., Soubiran, C., Masseron, T., Hawkins, K., Adibekyan, V., Buder, S., Casamiquela, L., Gilmore, G., Hourihane, A., and Tabernero, H. (2017b). Gaia FGK benchmark stars: opening the black box of stellar element abundance determination. A&A, 601:A38.

Jofré, P., Jackson, H., and Tucci Maia, M. (2020). Traits for chemical evolution in solar twins. Trends of neutron-capture elements with stellar age. A&A, 633:L9.

Jönsson, H., Allende Prieto, C., Holtzman, J. A., Feuillet, D. K., Hawkins, K., Cunha, K., Mészáros, S., Hasselquist, S., Fernández-Trincado, J. G., García-Hernández, D. A., Bizyaev, D., Carrera, R., Majewski, S. R., Pinsonneault, M. H., Shetrone, M., Smith, V., Sobeck, J., Souto, D., Stringfellow, G. S., Teske, J., and Zamora, O. (2018). APOGEE Data Releases 13 and 14: Stellar Parameter and Abundance Comparisons with Independent Analyses. AJ, 156(3):126.

Karakas, A. I. and Lattanzio, J. C. (2014). The Dawes Review 2: Nucleosynthesis and Stellar Yields of Low- and Intermediate-Mass Single Stars. PASA, 31:e030.

Kelson, D. D. (2003). Optimal Techniques in Two-dimensional Spectroscopy: Background Subtraction for the 21st Century. PASP, 115(808):688–699.

Kelson, D. D., Illingworth, G. D., van Dokkum, P. G., and Franx, M. (2000). The Evolution of Early-Type Galaxies in Distant Clusters. II. Internal Kinematics of 55 Galaxies in the z=0.33 Cluster CL 1358+62. ApJ, 531(1):159–183.

Kjeldsen, H. and Bedding, T. R. (1995). Amplitudes of stellar oscillations: the implications for asteroseismology. A&A, 293:87–106.

Kos, J., Bland-Hawthorn, J., Buder, S., Nordlander, T., Spina, L., Beeson, K. L., Lind, K., Asplund, M., Freeman, K., Hayden, M. R., Lewis, G. F., Martell, S. L., Sharma, S., De Silva, G., Simpson, J. D., Zucker, D. B., Zwitter, T., Čotar, K., Horner, J., Ting, Y.-S., and Traven, G. (2021). The GALAH survey: Chemical homogeneity of the Orion complex. MNRAS, 506(3):4232–4250.

Kouwenhoven, M. B. N., Goodwin, S. P., Parker, R. J., Davies, M. B., Malmberg, D., and Kroupa, P. (2010). The formation of very wide binaries during the star cluster dissolution phase. MNRAS, 404(4):1835–1848.

Kraus, A. L. and Hillenbrand, L. A. (2009). The Coevality of Young Binary Systems. ApJ, 704(1):531–547.

Krumholz, M. R., McKee, C. F., and Bland-Hawthorn, J. (2019). Star Clusters Across Cosmic Time. ARA&A, 57:227–303.

Lee, J.-E., Lee, S., Dunham, M. M., Tatematsu, K., Choi, M., Bergin, E. A., and Evans, N. J. (2017). Formation of wide binaries by turbulent fragmentation. *Nature Astronomy*, 1:0172.

Liu, F., Bitsch, B., Asplund, M., Liu, B.-B., Murphy, M. T., Yong, D., Ting, Y.-S., and Feltzing, S. (2021). Detailed elemental abundances of binary stars: searching for signatures of planet formation and atomic diffusion. MNRAS, 508(1):1227–1240.

Liu, F., Yong, D., Asplund, M., Feltzing, S., Mustill, A. J., Meléndez, J., Ramírez, I., and Lin, J. (2018). Detailed chemical compositions of the wide binary HD 80606/80607: revised stellar properties and constraints on planet formation. A&A, 614:A138.

Lodders, K. (2003). Solar System Abundances and Condensation Temperatures of the Elements. ApJ, 591(2):1220–1247.

Lu, H.-p., Karoff, C., and Zhang, L.-y. (2021). Magnetic activity and age estimation of red giants using neural networks. MNRAS, 505(2):2124–2135.

M. Kovalev, S. Brinkmann, M. Bergemann, and MPIA IT-department (2018). NLTE MPIA web server, [Online]. Available: http://nlte.mpia.de Max Planck Institute for Astronomy, Heidelberg.

Mack, Claude E., I., Schuler, S. C., Stassun, K. G., and Norris, J. (2014). Detailed Abundances of Planet-hosting Wide Binaries. I. Did Planet Formation Imprint Chemical Signatures in the Atmospheres of HD 20782/81? ApJ, 787(2):98.

Maia, M. T., Meléndez, J., Lorenzo-Oliveira, D., Spina, L., and Jofré, P. (2019). Revisiting the 16 Cygni planet host at unprecedented precision and exploring automated tools for precise abundances. A&A, 628:A126.

Masseron, T., Merle, T., and Hawkins, K. (2016). BACCHUS: Brussels Automatic Code for Characterizing High accUracy Spectra.

Meléndez, J., Asplund, M., Gustafsson, B., and Yong, D. (2009). The Peculiar Solar Composition and Its Possible Relation to Planet Formation. ApJ, 704(1):L66–L70.

Meléndez, J., Bergemann, M., Cohen, J. G., Endl, M., Karakas, A. I., Ramírez, I., Cochran, W. D., Yong, D., MacQueen, P. J., Kobayashi, C., and Asplund, M. (2012). The remarkable solar twin HIP 56948: a prime target in the quest for other Earths. A&A, 543:A29.

Nelson, T., Ting, Y.-S., Hawkins, K., Ji, A., Kamdar, H., and El-Badry, K. (2021). Distant Relatives: The Chemical Homogeneity of Comoving Pairs Identified in Gaia. *arXiv e-prints*, page arXiv:2104.12883.

Ness, M., Rix, H. W., Hogg, D. W., Casey, A. R., Holtzman, J., Fouesneau, M., Zasowski, G., Geisler, D., Shetrone, M., Minniti, D., Frinchaboy, P. M., and Roman-Lopes, A. (2018). Galactic Doppelgängers: The Chemical Similarity Among Field Stars and Among Stars with a Common Birth Origin. ApJ, 853(2):198.

Ness, M. K., Johnston, K. V., Blancato, K., Rix, H. W., Beane, A., Bird, J. C., and Hawkins, K. (2019). In the Galactic Disk, Stellar [Fe/H] and Age Predict Orbits and Precise [X/Fe]. ApJ, 883(2):177.

Nissen, P. E. (2015). High-precision abundances of elements in solar twin stars. Trends with stellar age and elemental condensation temperature. A&A, 579:A52.

Nissen, P. E., Christensen-Dalsgaard, J., Mosumgaard, J. R., Silva Aguirre, V., Spitoni, E., and Verma, K. (2020). High-precision abundances of elements in solar-type stars. Evidence of two distinct sequences in abundance-age relations. A&A, 640:A81.

Nissen, P. E. and Gustafsson, B. (2018). High-precision stellar abundances of the elements: methods and applications. A&A Rev., 26(1):6.

Nomoto, K., Kobayashi, C., and Tominaga, N. (2013). Nucleosynthesis in Stars and the Chemical Enrichment of Galaxies. ARA&A, 51(1):457–509.

Oh, S., Price-Whelan, A. M., Brewer, J. M., Hogg, D. W., Spergel, D. N., and Myles, J. (2018). Kronos and Krios: Evidence for Accretion of a Massive, Rocky Planetary System in a Comoving Pair of Solar-type Stars. ApJ, 854(2):138.

Oh, S., Price-Whelan, A. M., Hogg, D. W., Morton, T. D., and Spergel, D. N. (2017). Comoving Stars in Gaia DR1: An Abundance of Very Wide Separation Comoving Pairs. AJ, 153(6):257.

Pace, G., Melendez, J., Pasquini, L., Carraro, G., Danziger, J., François, P., Matteucci, F., and Santos, N. C. (2009). An investigation of chromospheric activity spanning the Vaughan-Preston gap: impact on stellar ages. A&A, 499(1):L9–L12.

Paxton, B., Marchant, P., Schwab, J., Bauer, E. B., Bildsten, L., Cantiello, M., Dessart, L., Farmer, R., Hu, H., Langer, N., Townsend, R. H. D., Townsley, D. M., and Timmes, F. X. (2015). Modules for Experiments in Stellar Astrophysics (MESA): Binaries, Pulsations, and Explosions. ApJS, 220(1):15.

Peñarrubia, J. (2021). Creation/destruction of ultra-wide binaries in tidal streams. MNRAS, 501(3):3670–3686.

Price-Jones, N. and Bovy, J. (2019). Blind chemical tagging with DBSCAN: prospects for spectroscopic surveys. MNRAS, 487(1):871–886.

Price-Jones, N., Bovy, J., Webb, J. J., Allende Prieto, C., Beaton, R., Brownstein, J. R., Cohen, R. E., Cunha, K., Donor, J., Frinchaboy, P. M., García-Hernández, D. A., Lane, R. R., Majewski, S. R., Nidever, D. L., and Roman-Lopes, A. (2020). Strong chemical tagging with APOGEE: 21 candidate star clusters that have dissolved across the Milky Way disc. MNRAS, 496(4):5101–5115.

Ramírez, I., Khanal, S., Aleo, P., Sobotka, A., Liu, F., Casagrande, L., Meléndez, J., Yong, D., Lambert, D. L., and Asplund, M. (2015). The Dissimilar Chemical Composition of the Planet-hosting Stars of the XO-2 Binary System. ApJ, 808(1):13.

Ramírez, I., Khanal, S., Lichon, S. J., Chanamé, J., Endl, M., Meléndez, J., and Lambert, D. L. (2019). The chemical composition of HIP 34407/HIP 34426 and other twin-star comoving pairs. MNRAS, 490(2):2448–2457.

Ramírez, I., Meléndez, J., and Asplund, M. (2009). Accurate abundance patterns of solar twins and analogs. Does the anomalous solar chemical composition come from planet formation? A&A, 508(1):L17–L20.

Ramírez, I., Meléndez, J., Bean, J., Asplund, M., Bedell, M., Monroe, T., Casagrande, L., Schirbel, L., Dreizler, S., Teske, J., Tucci Maia, M., Alves-Brito, A., and Baumann, P. (2014). The Solar Twin Planet Search. I. Fundamental parameters of the stellar sample. A&A, 572:A48.

Reggiani, H. and Meléndez, J. (2018). Evidences of extragalactic origin and planet engulfment in the metal-poor twin pair HD 134439/HD 134440. MNRAS, 475(3):3502–3510.

Rocha-Pinto, H. J., Castilho, B. V., and Maciel, W. J. (2002). Chromospherically young, kinematically old stars. A&A, 384:912–924.

Röser, S. and Schilbach, E. (2019). Praesepe (NGC 2632) and its tidal tails. A&A, 627:A4.

Röser, S., Schilbach, E., and Goldman, B. (2019). Hyades tidal tails revealed by Gaia DR2. A&A, 621:L2.

Saffe, C., Flores, M., Jaque Arancibia, M., Buccino, A., and Jofré, E. (2016). Temperature condensation trend in the debris-disk binary system ζ^2 Reticuli. A&A, 588:A81.

Saffe, C., Jofré, E., Martioli, E., Flores, M., Petrucci, R., and Jaque Arancibia, M. (2017). Signatures of rocky planet engulfment in HAT-P-4. Implications for chemical tagging studies. A&A, 604:L4.

Silva Aguirre, V., Davies, G. R., Basu, S., Christensen-Dalsgaard, J., Creevey, O., Metcalfe, T. S., Bedding, T. R., Casagrande, L., Handberg, R., Lund, M. N., Nissen, P. E., Chaplin, W. J., Huber, D., Serenelli, A. M., Stello, D., Van Eylen, V., Campante, T. L., Elsworth, Y., Gilliland, R. L., Hekker, S., Karoff, C., Kawaler, S. D., Kjeldsen, H., and Lundkvist, M. S. (2015). Ages and fundamental properties of Kepler exoplanet host stars from asteroseismology. MNRAS, 452(2):2127–2148.

Skúladóttir, Á., Hansen, C. J., Salvadori, S., and Choplin, A. (2019). Neutron-capture elements in dwarf galaxies. I. Chemical clocks and the short timescale of the r-process. A&A, 631:A171.

Skumanich, A. (1972). Time Scales for Ca II Emission Decay, Rotational Braking, and Lithium Depletion. ApJ, 171:565.

Sneden, C., Bean, J., Ivans, I., Lucatello, S., and Sobeck, J. (2012). MOOG: LTE line analysis and spectrum synthesis.

Sneden, C. A. (1973). *Carbon and Nitrogen Abundances in Metal-Poor Stars.* PhD thesis, The University of Texas at Austin.

Soderblom, D. R. (2010). The Ages of Stars. ARA&A, 48:581–629.

Spina, L., Meléndez, J., Karakas, A. I., Ramírez, I., Monroe, T. R., Asplund, M., and Yong, D. (2016). Nucleosynthetic history of elements in the Galactic disk. [X/Fe]-age relations from high-precision spectroscopy. A&A, 593:A125.

Tanaka, M., Utsumi, Y., Mazzali, P. A., Tominaga, N., Yoshida, M., Sekiguchi, Y., Morokuma, T., Motohara, K., Ohta, K., Kawabata, K. S., Abe, F., Aoki, K., Asakura, Y., Baar, S., Barway, S., Bond, I. A., Doi, M., Fujiyoshi, T., Furusawa, H., Honda, S., Itoh, Y., Kawabata, M., Kawai, N., Kim, J. H., Lee, C.-H., Miyazaki, S., Morihana, K., Nagashima, H., Nagayama, T., Nakaoka, T., Nakata, F., Ohsawa, R., Ohshima, T., Okita, H., Saito, T., Sumi, T., Tajitsu, A., Takahashi, J., Takayama, M., Tamura, Y., Tanaka, I., Terai, T., Tristram, P. J., Yasuda, N., and Zenko, T. (2017). Kilonova from post-merger ejecta as an optical and near-Infrared counterpart of GW170817. PASJ, 69(6):102.

Teske, J. K., Ghezzi, L., Cunha, K., Smith, V. V., Schuler, S. C., and Bergemann, M. (2015). Abundance Differences between Exoplanet Binary Host Stars XO-2N and XO-2S—Dependence on Stellar Parameters. ApJ, 801(1):L10.

Teske, J. K., Khanal, S., and Ramírez, I. (2016). The Curious Case of Elemental Abundance Differences in the Dual Hot Jupiter Hosts WASP-94A and B. ApJ, 819(1):19.

Thielemann, F. K., Arcones, A., Käppeli, R., Liebendörfer, M., Rauscher, T., Winteler, C., Fröhlich, C., Dillmann, I., Fischer, T., Martinez-Pinedo, G., Langanke, K., Farouqi, K., Kratz, K. L., Panov, I., and Korneev, I. K. (2011). What are the astrophysical sites for the r-process and the production of heavy elements? *Progress in Particle and Nuclear Physics*, 66(2):346–353.

Titarenko, A., Recio-Blanco, A., de Laverny, P., Hayden, M., and Guiglion, G. (2019). The AMBRE Project: [Y/Mg] stellar dating calibration with Gaia. A&A, 622:A59.

Tokovinin, A. (2017). Formation of wide binary stars from adjacent cores. MNRAS, 468(3):3461–3467.

van de Voort, F., Quataert, E., Hopkins, P. F., Kereš, D., and Faucher-Giguère, C.-A. (2015). Galactic r-process enrichment by neutron star mergers in cosmological simulations of a Milky Way-mass galaxy. MNRAS, 447(1):140–148.

Winteler, C., Käppeli, R., Perego, A., Arcones, A., Vasset, N., Nishimura, N., Liebendörfer, M., and Thielemann, F. K. (2012). Magnetorotationally Driven Supernovae as the Origin of Early Galaxy r-process Elements? ApJ, 750(1):L22.

Yong, D., Kobayashi, C., Da Costa, G. S., Bessell, M. S., Chiti, A., Frebel, A., Lind, K., Mackey, A. D., Nordlander, T., Asplund, M., Casey, A. R., Marino, A. F., Murphy, S. J., and Schmidt, B. P. (2021). r-Process elements from magnetorotational hypernovae. Nature, 595(7866):223–226.

Zhang, H. W., Gehren, T., and Zhao, G. (2008). A non-local thermodynamic equilibrum study of scandium in the Sun. A&A, 481(2):489–497.